THE UNIVERSITY OF MISSOURI

Bulletin

ENGINEERING REPRINT SERIES

Reprint Number 40

Engineering Experiment Station

Columbia, Missouri

A. APPLICATION OF THE SMITH CHART TO THE DESIGN OF MICROWAVE ABSORBING MATERIALS

D. L. Waidelich

Professor of Electrical Engineering

University of Missouri

B. SYNTHESIS OF CONTROL SYSTEMS BASED ON AN APPROXIMATION TO A THIRD-ORDER SYSTEM

C. R. Hausenbauer

University of Arizona

Tucson, Ariz.

G. V. Lago

Professor of Electrical Engineering

University of Missouri

Columbia, Missouri

COLLEGE OF ENGINEERING
THE ENGINEERING EXPERIMENT STATION

The Engineering Experiment Station was organized in 1909 as a part of the College of Engineering. The staff of the Station includes all members of the Faculty of the College of Engineering, together with Research Assistants supported by the Station Funds.

The Station is primarily an engineering research institution engaged in the investigation of fundamental engineering problems of general interest, in the improvement of engineering design, and in the development of new industrial processes.

The Station desires particularly to co-operate with industries of Missouri in the solution of such problems. For this purpose, there is available not only the special equipment belonging to the Station but all of the equipment and facilities of the College of Engineering not in immediate use for class instruction.

Inquiries regarding these matters should be addressed to

The Director,
Engineering Experiment Station
University of Missouri
Columbia, Missouri

THE UNIVERSITY OF MISSOURI BULLETIN

VOL. 60, NO. 1 ENGINEERING REPRINT SERIES, NO. 40

Published by the University of Missouri at Publications Office, Columbia, Missouri. Entered as second-class matter, January 2, 1914, at post office at Columbia, Missouri, under Act of Congress of August 24, 1912. Issued four times monthly October through May, three times monthly June through September.

500

January 1, 1959

Application of the Smith Chart to the Design of Microwave Absorbing Materials*

by D. L. Waidelich
University of Missouri

Abstract: Microwave absorbing materials are employed in the testing of radiating devices particularly when the space available is restricted. The Smith Chart has been found useful in the design of these absorbing materials but one of the major problems in the use of the Smith Chart for this application is the fact that the lossy dielectrics used may have a complex characteristic impedance. The Smith Chart as usually used assumes that the characteristic impedance is a real number. The modifications necessary in the use of the Smith Chart for complex characteristic impedances are given. Also, a graphical method of using another type of impedance chart together with the Smith Chart has been developed and is presented.

In the design solutions presented it is assumed that both the permeability and permittivity of the dielectrics are complex numbers and that the plane electromagnetic waves are normally incident upon the dielectric. The design of a one-layer, two-layer and multi-layer absorbing material is given. Also, a design solution for an absorber using conducting films as well as absorbing dielectric layers is presented.

Introduction:

The Smith chart has been very useful in the solution of problems using lossless transmission lines[1] and recently it has been applied to general two terminal-pair networks.[2] The use of the Smith chart has also been found advantageous in the determination of the transmission characteristics of plane electromagnetic waves in sandwich structures.[3] It was believed that the Smith chart might be found useful in the problem of plane wave propagation in microwave absorbing materials.[4] The purpose of this paper is to indicate how the chart might be applied in this problem and to solve some sample problems involving one or more layers of different dielectrics and conducting films.

One of the major problems encountered in using the Smith chart for a lossy dielectric is the fact that the characteristic impedance is a complex number. One method of using a complex characteristic impedance has been presented.[2] A different method is presented here involving the use of a Carter chart along with the Smith chart.

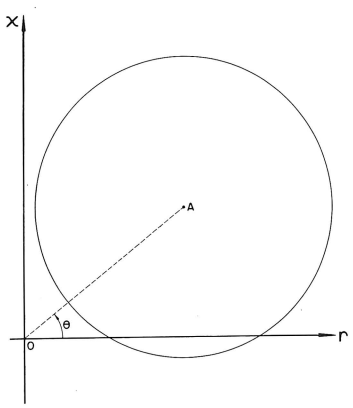

Fig. 1

A Constant Attenuation Circle

$\overline{OA} = |\coth 2\alpha y|$

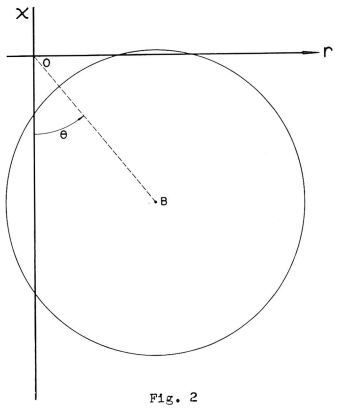

Fig. 2

A Constant Phase Shift Circle

$\overline{OB} = |\cot 2\beta y|$

*Much of the work reported here was performed at a classified government facility.

The Complex Characteristic Impedance:

To develop the theory for a chart[5] involving a complex characteristic impedance, let it be supposed that a transmission line short circuited at the receiving end is employed. The line has a characteristic impedance $Z_0 \angle \theta$ and a propagation constant $\gamma = \alpha + j\beta$. The impedance at any point y units from the receiving end is

$$Z = Z_0 \angle \theta \tanh \gamma y \qquad (1)$$

where $Z = R + jX$. If $r = (R/Z_0)$ and $x = (X/Z_0)$, then it is possible to show that the locus of constant attenuation (αy) in the r - x plane is a circle of

$$\text{center} = (\cos\theta \coth 2\alpha y, \sin\theta \coth 2\alpha y) \qquad (2)$$

and

$$\text{radius} = \frac{1}{|\sinh 2\alpha y|} . \qquad (3)$$

The details are given in the Appendix. A picture of a typical circle is shown in Fig. 1, and all of the other circles of the family will have centers along the line OA.

In a similar fashion the locus of constant phase shift (βy) in the r - x plane is a circle of

$$\text{center} = (\sin\theta \cot 2\beta y, -\cos\theta \cot 2\beta y) \qquad (4)$$

$$\text{and radius} = \frac{1}{|\sin 2\beta y|} . \qquad (5)$$

A picture of a typical circle is shown in Fig. 2, and all of the other circles of the family will have centers along the line OB.

The two families of circles as illustrated in Figs. 1 and 2 are exactly the same as those used in the usual rectangular impedance chart[5] except that the axes on which the centers lie are rotated counterclockwise through an angle of θ degrees. Thus in Fig. 3 if r' and x' are the axes of the usual rectangular chart, the actual axes r and x representing normalized resistance and reactance are rotated clockwise through an angle θ as shown in Fig. 3. The axes r and x are those used for a system having a complex characteristic impedance of angle θ.

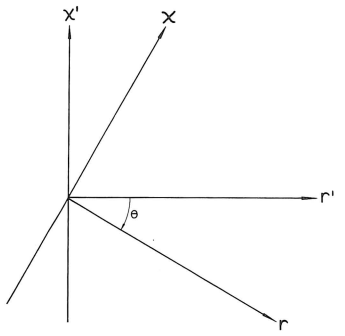

Fig. 3

The two sets of axes of a rectangular impedance chart.

The usual rectangular impedance chart suffers from the disadvantage of requiring an infinite half plane for displaying all of the necessary impedance points. All of these impedance points can be displayed within a circle of finite radius by use of the transformation[6] that changes the rectangular impedance chart into the Smith chart. As shown in the Appendix the r axis of Fig. 3 becomes the circle of center

$$(0, \cot\theta) \qquad (6)$$

$$\text{and radius } \frac{1}{|\sin\theta|} \qquad (7)$$

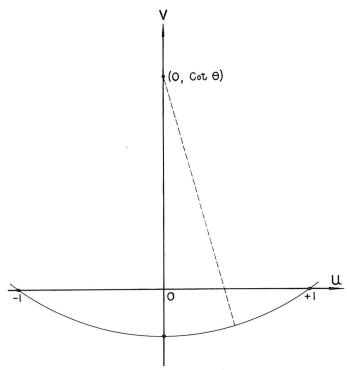

Fig. 4

The circle corresponding to the r axis of Figure 3.

$$\text{Radius} = \frac{1}{|\sin\theta|}$$

on the u - v plane of the Smith chart where $\rho = u + jv$. This circle is shown in Fig. 4, and the points -1, 0, +1 on the u-axis correspond to the points 0, 1, ∞ of the Smith chart. As the angle θ approaches zero the circle approaches the u axis. As θ approaches ninety degrees the circle becomes one of unit radius about the origin as a center. In a similar manner the x axis of Fig. 3 becomes the circle of center

$$(0, -\tan\theta) \qquad (8)$$

$$\text{and radius } \frac{1}{|\cos\theta|} \qquad (9)$$

on the u - v plane of the Smith chart. This circle is shown in Fig. 5. As the angle θ approaches zero, the circle approaches a circle of unit radius about the origin. As the angle θ approaches ninety degrees, the circle approaches the u - axis.

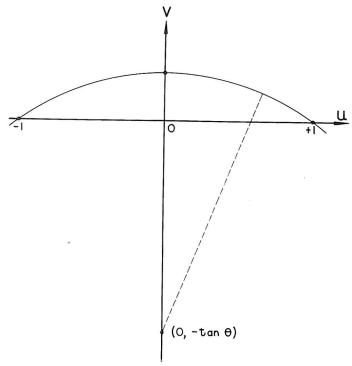

Fig. 5

The circle corresponding to the x axis of Figure 3.

$$\text{Radius} = \frac{1}{|\cos\theta|}$$

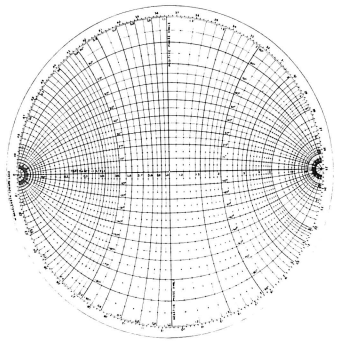

Fig. 6

The bi-polar or Carter chart.

The chart[7,8] described by the circles of (6), (7), (8) and (9) is shown in Fig. 6. The chart might be called the bi-polar[9] or Carter[7] chart and from this point on in this paper it will be referred to as the Carter chart. These charts are available commercially.[10] In the usual rectangular chart, points at a constant distance from the origin become circles crossing the u axis of Fig. 5 at right angles. In the Appendix it is shown that these circles have a center

$$\left(\frac{a^2 + 1}{a^2 - 1}, 0\right) \qquad (10)$$

$$\text{and a radius } \frac{2a}{|a^2 - 1|} \qquad (11)$$

These are the circles of Fig. 6 orthogonal to the circles of (6), (7), (8) and (9). Notice that $a = 0$ is the point (-1) on the u-axis, while $a \longrightarrow \infty$ is the point (+1) on the u-axis. Also $a = 1$ is the v axis. With the Carter chart of Fig. 6 available plus a Smith chart, it is possible to solve problems involving complex characteristic impedances.

In the actual use of the charts it was found that superimposing the Carter chart on the Smith chart was advantageous and one attempt at this is shown in Fig. 7. Since the phase shift circles (4) and (5) are the same as those of the Smith chart, the wavelength graduations on the chart may be used without change. Similarly the attenuation circles of (2) and (3) are the same as those of the Smith chart. For attenuation it is convenient to know that the attenuation circles cross the r' axis at $\coth \alpha y$ and $\tanh \alpha y$. To obtain αy, let w = the change in wavelengths. Then

$$\alpha y = \left(\frac{\alpha}{\beta}\right)(\beta y) = \left(\frac{\alpha}{\beta}\right) 2\pi w. \qquad (12)$$

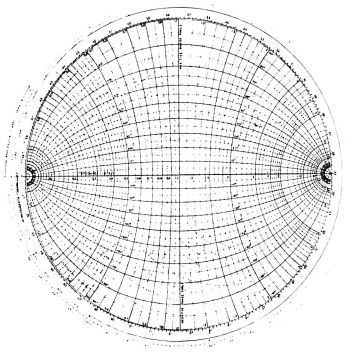

Fig. 7

Carter chart superimposed upon a Smith chart.

Application to Absorbing Materials:

The constants of materials suitable for microwave absorbing material may be expressed in terms of a complex permeability and a complex permittivity. Using MKS units the permeability μ is

$$\mu = \mu_o(\mu' - j\mu'') = \mu_o\mu'(1 - j\tan\delta_\mu) \qquad (13)$$

where $\mu_o = 4\pi \times 10^{-7}$
μ' = real part of normalized permeability
μ'' = imaginary part of normalized permeability
$\tan\delta_\mu = (\mu''/\mu')$ = magnetic dissipation factor

In a similar manner, the permittivity ϵ is

$$\epsilon = \epsilon_o(\epsilon' - j\epsilon'') = \epsilon_o\epsilon'(1 - j\tan\delta_\epsilon) \qquad (14)$$

where $\epsilon_o = (1/36\pi) \times 10^{-9}$
ϵ' = real part of normalized permittivity
ϵ'' = imaginary part of normalized permittivity
$\tan\delta_\epsilon = (\epsilon''/\epsilon')$ = electric dissipation factor

Assume also that plane electromagnetic waves are incident normally on a plane surface of the dielectric absorbing material. Then a transmission line analogy may be used and the intrinsic impedance of the dielectric is

$$\sqrt{\frac{\mu}{\epsilon}} = \sqrt{\frac{\mu_o\mu'(1 - j\tan\delta_\mu)}{\epsilon_o\epsilon'(1 - j\tan\delta_\epsilon)}} = \sqrt{\frac{\mu_o}{\epsilon_o}}\ \eta\ \angle\theta \qquad (15)$$

The propagation constant of the dielectric is

$$\alpha + j\beta = \sqrt{\alpha^2 + \beta^2}\ \angle\varphi = j\omega\sqrt{\mu_o\mu'(1 - j\tan\delta_\mu)\,\epsilon_o\epsilon'(1 - j\tan\delta_\epsilon)} \qquad (16)$$

where $\omega = 2\pi f = 2\pi$(frequency).
From (15) and (16):

$$\sqrt{\alpha^2 + \beta^2} = \frac{2\pi}{\lambda}\sqrt{\frac{\mu'\epsilon'}{(\cos\delta_\mu)(\cos\delta_\epsilon)}} \qquad (17)$$

where $\lambda = (1/f\sqrt{\mu_o\epsilon_o})$

$$\eta = \sqrt{\frac{\mu'}{\epsilon'}}\sqrt{\frac{\cos\delta_\epsilon}{\cos\delta_\mu}} \qquad (18)$$

$$\varphi = \frac{\pi}{2} - \frac{1}{2}(\delta_\epsilon + \delta_\mu) \qquad (19)$$

and $$\theta = \frac{1}{2}(\delta_\epsilon - \delta_\mu) \qquad (20)$$

As a first example of the use of the charts, assume that a single-layer absorber is used with a metal backing as shown in Fig. 8. The problem is to match the impedance of the absorber to that of air and to determine the thickness and other constants of the absorber necessary to accomplish the matching. Assume that $(\beta_1/\alpha_1) = 5.0$ and that $\tan\delta_{\mu 1} = 0.0$ where the subscript 1 is for the single-layer absorber. From (16), (19) and (20), $\varphi_1 = 78.7^o$, $\delta_{\epsilon 1} = 22.6^o$, $\theta_1 = 11.3^o$. The combined chart of Fig. 7 is very useful here, and an outline of the operations performed on the chart is shown in Fig. 9. A series of points on the chart were determined as indicated in Table I. The values of αy were obtained by the use of (12) and the radius to each of the points A, B, C, ··· G from the center of the circle of Fig. 9, is the distance along the u axis from the center of the circle to the value of $\coth \alpha y$. The starting point A of Fig. 9 is the zero impedance (short circuit) of the perfect conductor. The end point is the point between F and G at which the spiral crosses the r axis which is the circle for $\theta_1 = 11.3^o$. This crossing point is 0.261 wavelength from the short circuit and for this point $r_1 = 3.04$, $x_1 = 0.0$. From (A-17) of the Appendix, $r_1' = 2.98$, $x_1' = -0.56$. For matching, from (15) and (18)

$$\sqrt{\frac{\mu_o}{\epsilon_o}} = r\sqrt{\frac{\mu_o}{\epsilon_o}}\,n_1 = \eta\sqrt{\frac{\mu_o}{\epsilon_o}}\sqrt{\frac{\mu_1'}{\epsilon_1'}}\sqrt{\frac{\cos\delta_{\epsilon 1}}{\cos\delta_{\mu 1}}} \qquad (21)$$

or $$\sqrt{\frac{\mu_1'}{\epsilon_1'}} = \frac{1}{r}\sqrt{\frac{\cos\delta_{\mu 1}}{\cos\delta_{\epsilon 1}}} = \frac{1}{3.04}\sqrt{\frac{\cos 0^o}{\cos 22.6^o}} = 0.342$$

Table I
Series of Points for Figure 9

Point	w (wavelengths)	αy	$\coth \alpha y$
A	0.00	0.0000	∞
B	0.05	0.0628	15.97
C	0.10	0.1257	8.00
D	0.15	0.1885	5.37
E	0.20	0.2513	4.06
F	0.25	0.3142	3.29
G	0.30	0.3770	2.78

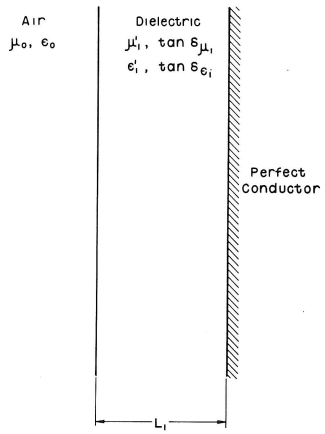

Fig. 8

Structure of a single-layer absorber.

Then if $\mu_1' = 1.0$, $\epsilon_1' = 8.6$. With these constants a perfect match would be achieved at this frequency. To determine the actual thickness of the dielectric obtain $\beta_1\lambda$ from (16) and (17).

$$\beta_1\lambda = (\sin\varphi_1)\sqrt{\frac{\mu_1'\epsilon_1'}{(\cos\delta_{\mu 1})(\cos\delta_{\epsilon 1})}} \qquad (22)$$

Using the above values for φ_1, μ_1', ϵ_1', $\delta_{\mu 1}$ and $\delta_{\epsilon 1}$, $\beta_1\lambda = 18.64$ wavelengths. Now $\beta_1 L_1 = 0.261$ wavelengths so $(L_1/\lambda) = .00877$. The wavelength λ is that of a plane wave in free space.

If the loss in the dielectric is very low (β_1/α_1 very high) the spiral of Fig. 9 approaches the center of the circle very slowly. Each time the spiral intersects the r axis (θ_1 = constant) another solution results. The solution with the thinnest dielectric, however, is the first solution, i.e., the same one as shown in Fig. 9. If, on the other hand, the loss in the dielectric is very high (β_1/α_1 very low) the spiral of Fig. 9 approaches the center of the circle very quickly. The approach may be so fast that no intersection with the r - axis exists and so no solution exists. Hence, if the loss in the dielectric is made too high, no solution results.

Since in transmission lines two quarter wavelength transformers in tandem have a wider band width than one transformer, it follows probably that a two-layer dielectric should have a wider band width than a single-layer one. Similarly, a n-layer dielectric should have a wider band width than a (n-1)-layer one. The cross section of a two layer dielectric is shown in Fig. 10. Assume for the first layer that $(\beta_1/\alpha_1) = 10.0$,

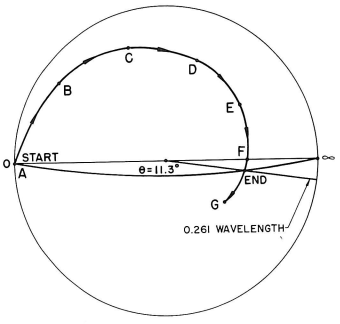

Fig. 9

Diagram of a chart showing solution for a single-layer absorber.

$\tan\delta_{\mu 1} = 0.0$, and $\beta_1 L_1 = 0.17$ wavelength. Fig. 11 shows the outline of the combined chart of Fig. 7 for the first layer. The point A at the start represents the short circuit of the perfect conductor. The point B at the end represents the position of the interface between the first and second dielectrics. For the point B, $r' = +0.46$ and $x' = +1.73$. The angles are calculated as $\varphi_1 = 84.29^o$, $\delta_{\epsilon 1} = 11.42^o$ and $\theta_1 = 5.71^o$. From (A-18)

$$r = +0.286,\ x = +1.77. \qquad (23)$$

For the second layer assume $(n_1/n_2) = 2.0$, $(\beta_2/\alpha_2) = 5.0$ and $\tan\delta_{\mu 2} = 0.0$, then $\varphi_2 = 78.7^o$, $\delta_{\epsilon 2} = 22.6^o$ and $\theta_2 = 11.3^o$. The r and x for the first layer as given in (23) must be changed into a new r and x for the second layer by using the ratio (n_1/n_2). Thus the new r and x are

$$r = (0.286)\left(\frac{n_1}{n_2}\right) = (0.286)(2.0) = 0.572 \qquad (24)$$

$$x = (1.77)(n_1/n_2) = (1.77)(2.0) = 3.54$$

From (A-17), $r' = 1.253$ and $x' = 3.358$. This point is shown as the starting point in Fig. 12. The end point is obtained at the crossing point of the spiral with the $\theta_2 = 11.3^o$ circle. At this end point $r' = 6.7$, $x' = -1.3$. From (A-18), $r = 6.8$, $x = 0.0$. For matching from (21)

$$\sqrt{\frac{\mu_2'}{\epsilon_2'}} = \frac{1}{(6.8)}\sqrt{\frac{\cos 0^o}{\cos 22.6^o}} = 0.1533 \qquad (25)$$

and if $\mu_2' = 1.0$, $\epsilon_2' = 42.6$. Also $n_2 = \frac{1}{6.8} = 0.1473$, $n_1 = 2(0.1473) = 0.2946$,

$$\sqrt{\frac{\mu_1'}{\epsilon_1'}} = (0.2946)\sqrt{\frac{\cos 0^o}{\cos 11.42^o}} = 0.2975 \qquad (26)$$

If $\mu_1' = 1.0$, $\epsilon_1' = 11.25$. From (22) $\beta_1\lambda = 3.36$ and since $\beta_1 L_1 = 0.17$, $(L_1/\lambda) = 0.0506$. Similarly $\beta_2\lambda = 6.64$, $\beta_2 L_2 = 0.047$ from Fig. 12 and $(L_2/\lambda) = 0.00708$. The results for the two-layer absorber are summarized in Table II. Non-magnetic dielectrics were assumed in this particular example although $\tan\delta_\mu$ could be assumed not zero and μ' greater than one without any additional trouble. The extension of this method to three or more layers is immediate.

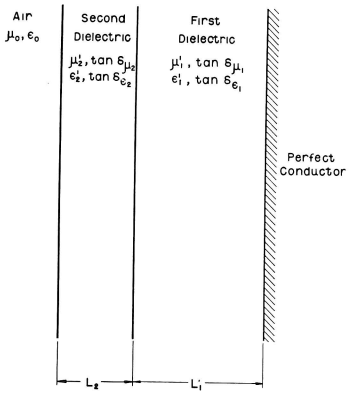

Fig. 10

Structure of a double-layer absorber.

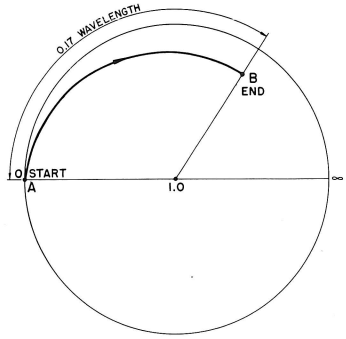

Fig. 11

Outline of chart for the first layer.

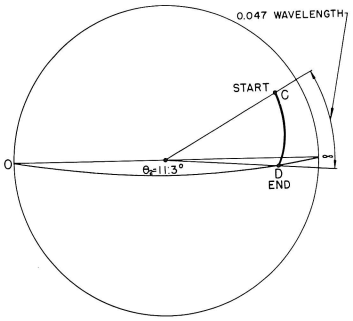

Fig. 12

Outline of chart for the second layer.

Conducting films on top of one dielectric layer or between two dielectric layers such as layers one and two of Fig. 10 may also be used to help in absorbing the plane waves. To indicate how such a film might be included in the calculations, suppose that a conducting film were placed on top of a single layer such as that of Fig. 8. The problem is to find the characteristics of the conducting layer so that matching occurs. Assuming $n_1 = 0.5$,

Table II

Results for the two-layer absorber

Layer	μ'	ϵ'	$\tan\delta_\mu$	$\tan\delta_\epsilon$	L/λ
First	1.0	11.25	0.0	0.202	0.0506
Second	1.0	42.6	0.0	0.416	0.00708

$\tan\delta_{\mu 1} = 0.0$, $(\beta_1/\alpha_1) = 10.0$ and $\beta_1 L_1 = 0.17$ wavelength, then from Fig. 11, $r' = +0.46$ and $x' = +1.73$. Also $\varphi_1 = 84.29^\circ$, $\delta_{\epsilon 1} = 11.42^\circ$ and $\theta_1 = 5.71^\circ$ and then $r = +0.286$ and $x = +1.77$. The normalized admittance Y_1 of the dielectric is then

$$Y_1 = \frac{1}{0.5(0.286 + j1.77)} = 0.178 - j1.103 \qquad (27)$$

The normalized admittance Y_f of the conducting film plus Y_1 must equal 1.0 + j0.0 if matching is to be accomplished. Then

$$Y_f = 0.822 + j1.103 \qquad (28)$$

The actual impedance of the required conducting film is (164 - j220) ohms for a square meter. Assuming $\mu_1 = 1.0$, from (18), $\epsilon_1 = 4.08$ and from (22), $\beta_1\lambda = 2.03$. Then $(L_1/\lambda) = 0.0837$.

Conclusions:

This paper presents a method utilizing the Smith and the Carter charts by which the constants of lossy dielectrics and conducting films may be determined so that matching may occur at the one frequency selected. No information has been presented, however, on the companion problems of optimizing the absorbing structure in particular directions such as those of thickness, weight or band width[4] or of synthesizing the lossy dielectrics and conducting films needed.

Appendix

Equations of the Circle Diagram

From (1):

$$R + jX = (Z_o \cos\theta + jZ_o \sin\theta)\tanh(\alpha + j\beta)y \qquad (A\text{-}1)$$
$$= (Z_o \cos\theta + jZ_o \sin\theta)\left(\frac{\sinh 2\alpha y + j\sin 2\beta y}{\cosh 2\alpha y + \cos 2\beta y}\right)$$

Normalizing (A-1) and separating real and imaginary parts:

$$r = \frac{R}{Z_o} = \frac{\cos\theta\sinh 2\alpha y - \sin\theta\sin 2\beta y}{\cosh 2\alpha y + \cos 2\beta y} \qquad (A\text{-}2)$$

$$x = \frac{X}{Z_o} = \frac{\sin\theta\sinh 2\alpha y + \cos\theta\sin 2\beta y}{\cosh 2\alpha y + \cos 2\beta y} \qquad (A\text{-}3)$$

From (A-2) and (A-3):

$$\cosh 2\alpha y + \cos 2\beta y = \frac{\sinh 2\alpha y}{r\cos\theta + x\sin\theta} = \frac{\sin 2\beta y}{-r\sin\theta + x\cos\theta} \qquad (A\text{-}4)$$

From the middle and right hand parts of (A-4):

$$(-r\sin\theta + x\cos\theta)^2 \cosh^2 2\alpha y + (r\cos\theta + x\sin\theta)^2 \cos^2 2\beta y = r^2 + x^2 \qquad (A\text{-}5)$$

From the left and right hand parts of (A-4):

$$(-r\sin\theta + x\cos\theta)^2 \cosh^2 2\alpha y = \sin^2 2\beta y - 2(-r\sin\theta + x\cos\theta)\sin 2\beta y \cos 2\beta y + (-r\sin\theta + x\cos\theta)\cos^2 2\beta y \qquad (A\text{-}6)$$

Eliminating $\cosh 2\alpha y$ between (A-5) and (A-6) gives

$$\tan 2\beta y = \frac{2(-r\sin\theta + x\cos\theta)}{(1 - r^2 - x^2)} \qquad (A\text{-}7)$$

Now let $D = \left[(1 - r^2 - x^2)^2 + 4(-r\sin\theta + x\cos\theta)\right]^{\frac{1}{2}}$

$$= \left[(1 + r^2 + x^2)^2 - 4(r\cos\theta + x\sin\theta)\right]^{\frac{1}{2}} \qquad (A\text{-}8)$$

Then from (A-7) and (A-8):

$$\sin 2\beta y = \frac{2}{D}(-r\sin\theta + x\cos\theta) \qquad (A\text{-}9)$$

$$\cos 2\beta y = \frac{1}{D}(1 - r^2 - x^2) \qquad (A\text{-}10)$$

From (A-4), (A-9) and (A-10):

$$\sinh 2\alpha y = \frac{2}{D}(r\cos\theta + x\sin\theta) \qquad (A\text{-}11)$$

$$\cosh 2\alpha y = \frac{1}{D}(1 + r^2 + x^2) \qquad (A\text{-}12)$$

$$\tanh 2\alpha y = \frac{2(r\cos\theta + x\sin\theta)}{(1 + r^2 + x^2)} \qquad (A\text{-}13)$$

Suppose now that (αy) is assumed constant. From (A-13):

$$(r - \cos\theta\coth 2\alpha y)^2 + (x - \sin\theta\coth 2\alpha y)^2 = \frac{1}{\sinh^2 2\alpha y} \qquad (A\text{-}14)$$

This is a circle of center and radius as indicated in (2) and (3).

Now assume that (βy) is constant. From (A-7):

$$(r - \sin\theta\cot 2\beta y)^2 + (x + \cos\theta\cot 2\beta y)^2 = \frac{1}{\sin^2 2\beta y} \qquad (A\text{-}15)$$

This is a circle of center and radius as indicated in (4) and(5).

The transformation [6] that will convert the usual rectangular impedance chart into the Smith Chart is

$$\rho = \frac{z' - 1}{z' + 1} \quad \text{or} \quad z' = \frac{1 + \rho}{1 - \rho} \qquad (A\text{-}16)$$

where $z' = r' + jx'$ and $\rho = u + jv$. The r' and x' are the real and imaginary parts of the impedance z' of the rectangular chart, while u and v are the real and imaginary parts of the complex number ρ used in plotting the Smith Chart. From Fig. 3

$$r' = r\cos\theta + x\sin\theta$$
$$x' = -r\sin\theta + x\cos\theta \qquad (A\text{-}17)$$

or

$$r = r'\cos\theta - x'\sin\theta$$
$$x = r'\sin\theta + x'\cos\theta \qquad (A\text{-}18)$$

From (A-16) and (A-17):

$$z' = r' + jx' = (r\cos\theta + x\sin\theta) + j(-r\sin\theta + x\cos\theta)$$

$$= \frac{1 + \rho}{1 - \rho} = \frac{(1 + u) + jv}{(1 - u) - jv} \qquad (A\text{-}19)$$

Eliminate r from (A-19):

$$\left(u - \frac{x}{\sin\theta + x}\right)^2 + \left(v - \frac{\cos\theta}{\sin\theta + x}\right)^2 = \frac{1}{(\sin\theta + x)^2} \qquad (A\text{-}20)$$

For the r axis, $x = 0$ and (A-20) becomes

$$u^2 + (v - \cot\theta)^2 = \frac{1}{(\sin\theta)^2} \qquad (A\text{-}21)$$

This is a circle on the u-v plane with the center given by (6) and the radius of (7). Eliminating x from (A-19):

$$\left(u - \frac{r}{\cos\theta + r}\right)^2 + \left(v + \frac{\sin\theta}{\cos\theta + r}\right)^2 = \frac{1}{(\cos\theta + r)^2} \qquad (A\text{-}22)$$

For the x axis, $r = 0$ and (A-22) becomes

$$u^2 + (v + \tan\theta)^2 = \frac{1}{(\cos\theta)^2} \qquad (A\text{-}23)$$

This is a circle on the u-v plane with the center given by (8) and the radius by (9).

Assume on a rectangular chart such as Fig. 3 that a circle of radius a exists about the origin. From (A-19)

$$r' + jx' = \frac{(1 + u) + jv}{(1 - u) - jv} \qquad (A\text{-}24)$$

and

$$r' - jx' = \frac{(1 + u) - jv}{(1 - u) + jv} \qquad (A\text{-}25)$$

From (A-24) and (A-25):

$$a^2 = r'^2 + x'^2 = \frac{(1 + u)^2 + v^2}{(1 - u)^2 + v^2} \qquad (A\text{-}26)$$

or

$$\left(u - \frac{a^2 + 1}{a^2 - 1}\right)^2 + v^2 = \frac{4a^2}{(a^2 - 1)^2} \qquad (A\text{-}27)$$

This is a family of circles with center and radius given by (10) and (11).

REFERENCES

1. Krauss, H. L., "Transmission Line Charts", Electrical Engineering, 68, 767, September, 1949.
2. Dawirs, H. N., "Application of the Smith Chart to General Impedance Transformations", Proceedings of the IRE, 45, 954, July, 1957.
3. Mathis, H. F., "Transmission Characteristics of Sandwiches", Transactions of the IRE, MTT-3,5 7, October, 1955.
4. Waidelich, D. L., "The Band-Width of a Single-Layer Microwave Absorbing Material". In preparation.
5. Jackson, W., "High Frequency Transmission Lines", John Wiley & Sons, New York, 1951, Chapter 6.
6. Reich, H. J., Ordung, P. F., Krauss, H. L., Skalnik, J. G., "Microwave Theory and Techniques", D. Van Nostrand Co., New York, 1953, pgs. 155, 856
7. Carter, P. S., "Charts for Transmission-Line Measurements and Computations", RCA Review, 3, 355 January, 1939.
8. Meinke, H. H., "Ein Kreisdiagramm zur Berechnung der Vorgange auf Leitungen", Hochfrequenztechnik und Elektroakustik, 57, 17, January, 1941.
9. Kimbark, E. W., "Electrical Transmission of Power and Signals", John Wiley and Sons, New York, 1949, page 187.
10. Carter charts are obtainable from the Industrial Products Division, International Telephone and Telegraph Corporation, 100 Kingsland Road, Clifton, New Jersey.
11. Ramo, S., and Whinnery, J. R., "Fields and Waves in Modern Radio", John Wiley and Sons, New York, Second Edition, 1953, Chapter 7.
12. Heizer, K. W., and Koepsel, W. W., "Studies Leading to the Development of an Electromagnetic Dark-room", Final Report, Navy Contract NOy-73242, Southern Methodist University, Dallas, Texas.

Transactions Paper

(Reviewed and Accepted for Publication)

SYNTHESIS OF CONTROL SYSTEMS BASED ON AN APPROXIMATION TO A THIRD-ORDER SYSTEM

C. R. Hausenbauer
Nonmember AIEE
University of Arizona
Tucson, Ariz.

G. V. Lago
Member AIEE
University of Missouri
Columbia, Mo.

A paper recommended by the AIEE Feedback Control Systems Committee and approved by the AIEE Technical Operations Department for presentation at the AIEE Summer General Meeting and Air Transportation Conference, Buffalo, N. Y., June 22-27, 1958. Manuscript submitted October 7, 1957; made available for printing April 14, 1958.

Price: 40¢ To Members
80¢ To Nonmembers

(5¢ per copy additional if first class mailing desired)

Paper No.
58-797

Discussion in Duplicate Due July 9, 1958.

SYNTHESIS OF CONTROL SYSTEMS BASED ON AN APPROXIMATION TO A THIRD-ORDER SYSTEM

*C. R. Hausenbauer
Nonmember AIEE

**G. V. Lago
Member AIEE

In recent years the high speed performance and accuracy demanded of military applications and industrial processes have placed increasing emphasis on the dynamic characteristics of control systems. However, system design is most effective when both steady-state and transient performance specifications can be realized. Ordinarily the designer works from the open-loop to the closed-loop, i.e., trial and error modifications are made to the fixed portion of the system until a compensation network is found that eventually leads to an acceptable closed-loop performance. In contrast, another approach, synthesis, proceeds from the closed-loop specifications to an appropriate open-loop system, which upon closure of the feedback path, satisfies the specifications. The methods of Guillemin[1] and Aaron[2] accomplish this transition, but not without difficulties and complications which arise from the fact that a closed-loop transfer function must be selected that simultaneously: (1) exhibits a pole-zero excess equal to or greater than the excess of the fixed portion of the system, and (2) satisfies a set of closed-loop specifications. Recently Aseltine[3] introduced an inverse-root locus method that graphically determines the open-loop pole locations from a given closed-loop pole-zero configuration. However, none of these methods provides a simple procedure indicating how a closed-loop transfer function can be formulated directly from a detailed set of transient and steady-state specifications. This paper presents a quick and accurate method of synthesizing a linear, continous, unity-feedback system from a set of specifications that eliminates the above disadvantages. Attention is confined to a type I system that is compensated by an RC realizable transfer function. To be RC realizable, the poles of this function must be simple on the negative real axis, the origin and infinity excluded, i.e., its pole-zero excess must be equal to or greater than zero.

THEORY OF THE METHOD

Terminology pertinent to the proposed method of synthesis is indicated in Figure 1; features of the method are as follows:

1. A progression from a set of closed-loop performance specifications to an appropriate open-loop transfer function.

2. A rapid and accurate formulation from a set of specifications of a closed-loop transfer function $C(s)/R(s)$ not dependent upon the pole-zero excess of the fixed portion of the system $G_2(s)$.

3. Elimination of graphical procedures to determine the poles of the open-loop transfer function $G(s)$.

****

*C. R. Hausenbauer is with the University of Arizona, Tucson, Arizona

**G. V. Lago is with the University of Missouri, Columbia, Missouri

This research was supported by a National Science Foundation grant.

4. A simple criterion which assures that the nonzero poles of G(s) are always on the negative real axis.

5. A criterion for placing a pole of G(s) at a particular frequency to obtain a simplified compensation transfer function $G_1(s)$.

6. Incorporation of the $G_2(s)$ pole-zero excess requirement in a modified compensation transfer function $G_1'(s)$ as the final step of the procedure.

7. In most cases an elimination of steady-state and transient response verification of the closed-loop specifications.

Of these seven features, the first five are realizable with the simple idealized system in Figure 1(A), idealized in the sense that $G_1(s)$ is not required to have a pole-zero excess equal to or greater than zero. Features six and seven are realized with the modified system in Figure 1(B), in which the modified compensation transfer function $G_1'(s)$ has the necessary pole-zero excess equal to or greater than zero for it to be RC realizable.

Figure 1(C) indicates the significance of this division of the features into distinct parts. The Bode plot for G(s) represents the steady-state frequency response characteristic of an open-loop transfer function, which upon closure of the feedback path meets the steady-state and transient performance specifications, regardless of the nature and complexity of the fixed portion of the system. Ordinarily a relatively simple form for G(s) will meet a wide variety of closed-loop specifications. The curve for the modified open-loop transfer function $G'(s)$ is identical to the one for G(s) from ω equal to zero up to some frequency above the crossover frequency. The deviation from the latter curve at high frequencies represents the action of the poles that must be added to $G_1(s)$, as a consequence of the pole-zero excess of $G_2(s)$, for $G_1(s)$ to be RC realizable. Use is made of the fact that the higher the frequency at which the deviation of the curves occurs, the smaller will be the effect of the added poles on the closed-loop performance of the system. As a result, consideration of the complexity of $G_2(s)$ can be delayed until the final step of the synthesis procedure, and except in a marginal situation, there is no need to determine the roots of the modified characteristic equation.

DEVELOPMENT OF THE METHOD

To arrive at a workable method of synthesis that incorporates the features noted above, simple correlations are required between open-loop poles and zeros on the one hand, and closed-loop performance specifications on the other. Since $G_1(s)$, or $G_1'(s)$ as appropriate, is to be RC realizable, criteria must be established to assure that the nonzero poles of G(s) are on the negative real axis for a prescribed set of closed-loop specifications. The specifications considered are:

1. K_v = velocity constant

2. BW = 0.707 bandwidth

3. γ = per cent overshoot to a unit-step-input

4. t_r = 10% - 90% rise time

5. t_d = 50% delay time

To provide a means of expressing these specifications in a form suitable to comparing systems having a complex conjugate pair of poles with an arbitrary undamped angular frequency of ω_n rad/sec, it is convenient to express transfer functions in terms of the normalized complex frequency $p = s/\omega_n = x+jy$. In effect, this transformation contracts all s-plane pole-zero positions by the factor $1/\omega_n$. Accordingly, the coordinates of the p-plane are nondimensional, and to the variable p there corresponds normalized time $t' = \omega_n t$, also nondimensional. The closed-loop specifications in normalized terminology become: (1) K_v/ω_n, (2) BW/ω_n, (3) γ %, (4) $t'_r = \omega_n t_r$, and (5) $t'_d = \omega_n t_d$. In many situations a high value of normalized velocity constant K_v/ω_n is desirable to assure that the steady-state error for a velocity input is small. Noise considerations and mechanical resonance of dynamical elements external to the feedback path require that an upper limit be placed on system bandwidth. This limit, together with the desirability of a high K_v/ω_n, suggested forming the K_v/BW ratio and incorporating it as a design criterion in the synthesis procedure.

Reference 4 presents detailed analyses of several forms of closed-loop transfer functions. The prototype of these systems is a simple second-order system that is successively made more complicated by the inclusion of a real zero, a real pole only, and lastly, both a real pole and zero. Of the four systems the last one includes all the advantages, and removes the disadvantages, of the first three systems both in regard to incorporating the features enumerated in the previous section and realizing an extensive variety of transient and steady-state specifications. Accordingly, the only closed-loop transfer function to be considered here is the one given by

$$\frac{C(s)}{R(s)} = \frac{\omega_n^2 p_3}{z_1} \frac{s + z_1}{(s + p_3)(s^2 + 2\gamma\omega_n s + \omega_n^2)}, \tag{1}$$

where p_3, z_1, and ω_n can be altered as required with the aid of the design curves to follow. In terms of the normalized complex frequency $p = s/\omega_n$, equation 1 becomes

$$\frac{C(p)}{R(p)} = \frac{m}{k} \frac{p + k}{(p + m)(p^2 + 2\gamma p + 1)}, \tag{2}$$

where $k = z_1/\omega_n$, $m = p_3/\omega_n$, and γ is confined to the interval $0 \leq \gamma \leq 1.0$; no restriction is placed on the sign of k, but m is only positive to assure that equation 2 represents an absolutely stable system. The pole-zero configuration of this function is given in Figure 2. The open-loop transfer function $G(p)$ is given by

$$G(p) = \frac{C(p)/R(p)}{1 - C(p)/R(p)} \tag{3}$$

which upon substitution of equation 2 yields

$$G(p) = \frac{m}{k} \frac{p+k}{p\left[p^2+(m+2\zeta)p + (1+2\zeta m - m/k)\right]}$$

$$= \frac{m}{k} \frac{p+k}{p(p + p_4)(p + p_5)} . \tag{4}$$

The nonzero poles of G(p) are real when the inequality

$$k \leq \frac{m}{1 - (\zeta - m/2)^2} \tag{5}$$

is satisfied; here k may be negative. The normalized velocity constant K_v/ω_n is obtained by substituting equation 4 in the definition

$$\frac{K_v}{\omega_n} = \lim_{p \to 0} p\, G(p) , \tag{6}$$

with the result that

$$\frac{K_v}{\omega_n} = \frac{1}{2\zeta - \frac{1}{m} - \frac{1}{k}} = \frac{m}{p_4\ p_5} . \tag{7}$$

For the assumptions that the closed-loop poles are in the left-half plane and the nonzero poles of G(p) are on the negative real axis, then m, p_4, and p_5 are all positive. Hence, regardless of the location of the zero of C(p)/R(p), the normalized velocity constant must be a positive quantity. Clearly then, for k positive it is necessary that k satisfy the inequality

$$k \geq \frac{m}{1 + 2\zeta m} \tag{8}$$

to assure a positive K_v/ω_n, whereas for negative values of k, K_v/ω_n is always positive. Therefore, if inequality 5 is satisfied to assure that the nonzero poles of G(p) are real, then satisfaction of inequality 8 guarantees two things: (1) the nonzero poles of G(p) reside on the negative real axis, and (2) K_v/ω_n is positive. For k positive, inequalities 5 and 8 can be combined into

$$\frac{m}{1 + 2\zeta m} \leq k \leq \frac{m}{1 - (\zeta - m/2)^2} . \tag{9}$$

Figure 3 illustrates the general nature of inequalities 5 and 9 for ζ considered a constant. In the allowable regions A,B,C, and D, the nonzero poles of G(p) are distinct and reside on the negative real axis, and K_v/ω_n is positive. However, for points exterior to or on the boundaries of these regions, the poles of G(p) are complex conjugates, second-order on the negative real axis, or both poles are not on the negative real axis.

Now to each point in an allowable region there corresponds a unique closed-loop steady-state response as well as a unique transient response for a specified driving function. More specifically, in terms of system specifications, there exists a unique positive normalized velocity constant given by equation 7, and hence a locus along which K_v/ω_n is a constant. These loci are obtained by rearranging equation 7 as

$$k = \frac{m}{1 + m\left(2\zeta - \frac{1}{K_v/\omega_n}\right)}, \qquad (10)$$

in which ζ is fixed and K_v/ω_n is treated as a constant. In region A, K_v/ω_n falls in the interval $1/2\zeta \leq K_v/\omega_n \leq \infty$ for all positive values of m and k. However in the other regions, it can be shown that K_v/ω_n is always less than $1/2\zeta$, with definite restrictions on the values of m and k. Since ζ is normally confined to the interval $0.4 < \zeta < 1.0$, regions B, C, and D are of lesser importance. Of the four regions, region A exhibits the most favorable features and widest degree of freedom relative to a system synthesis procedure. As a consequence, the remainder of the discussion and the design curves pertinent thereto are concerned with points along loci of K_v/ω_n equal to a constant in region A only. For this region it should be noted that the zero at (-k) in Figure 2 always resides between the real pole and the origin.

For a unit-step-input $\mu(t)$, R(s) in equation 1 is 1/s. Using the familiar scale change theorem[5] the closed-loop transient response corresponding to equation 2 is

$$c(t'/\omega_n) = 1 + E \exp(-mt') + F\left[\exp(-\zeta t')\right] \sin(\beta t' + \psi) \qquad (11)$$

in terms of the normalized time $t' = \omega_n t$. Expressions for E, F, β and ψ are given in Appendix A. Figure 4 shows several responses for movement along a line for $K_v/\omega_n = 10$ when $\zeta = 0.707$. For low values of m the response has a long delay time and a long-time-constant-tail; these features indicate the presence of an open-loop phase lag dipole in the vicinity of the origin of the p-plane. The closed-loop normalized bandwidth BW/ω_n is obtained from

$$BW/\omega_n = v^{1/2}, \qquad (12)$$

where the expression for v is given in Appendix A.

Figures 5, 6, and 7 set forth a graphical summary of the transient and steady-state performance characteristics of the transfer function given by equation 2. The curves in these figures were prepared using inequality 9 and equations 10, 11, and 12. These curves can be used to form a C(p)/R(p) given by equation 2, and hence a C(s)/R(s) defined by equation 1 once a value of ω_n is decided upon, from a set of closed-loop specifications. Each figure presents curves of γ, k, BW/ω_n, K_v/BW, t_r' and t_d' versus m along a line of constant K_v/ω_n when ζ is fixed at 0.5 or 0.707. Figure 7 is concerned with values of m between zero and 0.4; as such, curves in this figure are useful for integral dipole compensation. For any point, on any curve in all figures, the nonzero poles of G(p) are on the negative real axis.

In these figures, as m and k approach zero, the ratio m/k approaches unity, the pole and zero in effect cancel each other, and the system essentially reduces to a simple second-order system. To the extreme right of the figures where m is equal to eight, the real pole of C(p)/R(p) has only a slight influence on the system performance, and the system behavior is very similar to that of a second-order system with a real zero. As m approaches infinity, the system performance is precisely that of a second-order system with a zero. Asymptotic values of $\mathcal{S}$, 10k, and BW/ω_n are identified in the figures at m = 8.0 by dashed lines. For intermediate values of m in the interval $0 < m < 8.0$, a very extensive variety of closed-loop performance is obtainable. In view of the usual tolerances on system performance specifications, the curves presented here are probably sufficient and representative of situations normally encountered with minimum-phase transfer functions, i.e., overshoots between five and forty per cent, and normalized velocity constants in the range of one to infinity. It is interesting to note that a comparison of the data for $\mathcal{S} = 0.707$ in Figure 6D and Figure 6E for K_v/ω_n equal to ten and infinity respectively, reveals that there are no appreciable differences in system performance; for higher values of $\mathcal{S}$, performance differences are less pronounced.

The normalized version of the idealized series compensation transfer function $G_1(p)$ given by

$$G_1(p) = G(p)/G_2(p) \tag{13}$$

can be simplified provided one of the nonzero poles of the normalized fixed portion of the system can be incorporated in the expression for the open-loop transfer function G(p) when C(p)/R(p) is formed from the specifications. For a fixed value of $\mathcal{S}$ and an arbitrary K_v/ω_n, the poles of G(p) at (-p4) and (-p5), obtained from equation 4, are related to Figure 5, 6 and 7 by

$$p4 = (\mathcal{S} + m/2) - \left[(\mathcal{S} + m/2)^2 - (1 + 2\mathcal{S}m - m/k)\right]^{1/2} \tag{14}$$

and

$$p5 = (\mathcal{S} + m/2) + \left[(\mathcal{S} + m/2)^2 - (1 + 2\mathcal{S}\,m - m/k)\right]^{1/2}. \tag{15}$$

It is readily shown that the following inequalities apply to the situation considered here:

$$0 \leq p4 < k < p5 \leq \infty \tag{16}$$

and

$$0 \leq p4 \leq \frac{1}{K_v/\omega_n} \leq 2\mathcal{S} \leq p5 \leq \infty \quad . \tag{17}$$

Figure 8A illustrates the general nature of the inequalities in expression 17 as a function of m, whereas Figure 8B exhibits the same information as pole loci of G(p). Consistent with satisfying a set of closed-loop specifications within prescribed tolerances, it is often possible to choose values of $\mathcal{S}$ and K_v/ω_n such that a pole of G(p) can be positioned almost anywhere on the negative real axis to coincide with one of the poles of $G_2(p)$, and thereby obtain a simplified $G_1(p)$. Figures 9 and 10, based on equations 14 and 15, present curves of p4, p5, and k for the particular case of $\mathcal{S} = 0.707$ along lines of constant K_v/ω_n. When used in conjunction with Figures 6 and 7 respectively, it is often possible to quickly

form a $C(p)/R(p)$, to which there corresponds an open-loop transfer function $G(p)$ containing a pole that coincides with a pole of $G_2(p)$.

PROCEDURE OF THE METHOD

The following procedure is well suited to synthesize a system from a set of closed-loop specifications and a given fixed portion of the system $G_2(s)$:

1. The K_v/BW ratio is used to select an appropriate set of design curves and a suitable value of ω_n for the purpose of normalization.
2. The analytical expressions for $C(p)/R(p)$ and the idealized $G(p)$ are formed.
3. $G_2(s)$ is normalized to yield $G_2(p)$.
4. If possible within specifications, $G(p)$ of step 2 is altered to exhibit a pole of $G_2(p)$.
5. The required idealized compensation transfer function is found from $G_1(p) = G(p)/G_2(p)$.
6. If necessary, poles are added to $G_1(p)$ using a Bode plot as a guide; this yields $G_1'(p)$ the modified compensation transfer function.
7. $G_1'(p)$ is synthesized as an RC network, and unnormalized with $p = s/\omega_n$ to obtain the final compensation network.

ILLUSTRATIVE EXAMPLE

Suppose that the fixed portion of the system is given by

$$G_2(s) = \frac{16.875 \times 10^3}{s(s+30)(s+125)}, \qquad (18)$$

and that the closed-loop specifications are:

$BW \leq 35$ rad/sec $\qquad\qquad \gamma < 35$ per cent

$K_v \geq 140$/sec $\qquad\qquad t_d < 0.065$ seconds

The specifications require that the ratio K_v/BW be equal to or greater than four. Figure 6D for $K_v/\omega_n = 10$ and $\zeta = 0.707$ exhibits a design ratio $K_v/BW \geq 4.92$, a ratio $BW/\omega_n \leq 2.03$, and overshoots less than thirty five per cent for all values of m in equation 2. Selecting a design value of $K_v = 150$/sec, then from $K_v/\omega_n = 10$, $\omega_n = 15$ rad/sec; from $BW/\omega_n = 2.03$, $BW = 30.45$ rad/sec. Thus the specifications for K_v, BW, and γ can be realized by the curves in Figure 6D. Also since $t_d' = \omega_n t_d$, then the normalized delay time must satisfy $t_d' \leq 0.975$. The t_d' curve in Figure 6D indicates that this requirement is satisfied provided $m \geq 0.70$. Therefore it is clear, that independent of the complexity of $G_2(s)$, a wide variety of transfer functions described by equation 2 can be formed with an $\omega_n = 15$ rad/sec to meet all the above specifications using the curves in Figure 6D when $m \geq 0.70$.

By first normalizing $G_2(s)$ with respect to $\omega_n = 15$ rad/sec, and using Figure 9D it is possible, in this case, to choose a pole of $G(p)$ to coincide with a pole of $G_2(p)$, and thereby obtain an immediate simplification of $G_1(p)$. Upon normalization equation 18 becomes

$$G_2(p) = \frac{5}{p(p+2)\ (p+8.33)} \quad . \tag{19}$$

Equation 4 suggests selecting a value of $p_5 = 8.33$. For this value of p_5, the curves in Figure 9D yield $p_4 = 0.0842$, $k = 0.686$, and $m = 7.0$. Accordingly equations 2 and 4 become

$$\frac{C(p)}{R(p)} = 10.21 \frac{p + 0.686}{(p + 7)\ (p^2 + 1.414\ p + 1)} \tag{20}$$

and

$$G(p) = 10.21 \frac{p + 0.686}{p(p + 0.0842)\ (p + 8.33)} \quad . \tag{21}$$

The required idealized compensation transfer function is then found to be

$$G_1(p) = \frac{G(p)}{G_2(p)} = 2.04 \frac{(p + 0.686)\ (p + 2)}{p + 0.0842} \quad . \tag{22}$$

For the idealized system of equation 20, the transient response is almost identical to the curve for $m = 8.0$ in Figure 4. For $m = 7.0$, Figure 6D indicates an actual overshoot of twenty-two per cent.

As the final step of the procedure, the plus three pole-zero excess requirement of $G_2(p)$ must be satisfied to assure an RC realizable compensation transfer function $G_1'(p)$, by adding a pole to $G(p)$, such that the resulting modified open-loop transfer function $G'(p)$ yields a closed-loop performance within the specifications. A suitable location of $p = -12$ for the added pole, while maintaining a normalized velocity constant of $K_v/\omega_n = 10$, is quickly determined with the aid of a Bode plot of the magnitude of equation 21 for $G(p)$. This additional pole decreases the calculated phase margin of 57.43 degrees, corresponding to the known overshoot of 22 per cent, to 51 degrees. This small decrease in phase margin results in only a slight increase in overshoot because phase margins of more than 45 degrees are usually indicative of overshoots of 30 per cent or less.

Adding the pole at $p = -12$ to the idealized open-loop transfer function $G(p)$ of equation 21, while maintaining both K_v/ω_n and the position of the zero at $p = -0.686$, yields the normalized modified open-loop transfer function

$$G'(p) = 122.5 \frac{p + 0.686}{p\ (p + 0.0842)\ (p + 8.33)\ (p + 12)} \tag{23}$$

Applying the same technique to equation 22 gives the desired normalized modified series compensation transfer function

$$G_1'(p) = 24.48 \frac{(p + 0.686)\ (p + 2)}{(p + 0.0842)\ (p + 12)} \quad . \tag{24}$$

The unnormalized version of this result is

$$G_1'(s) = 24.48 \frac{(s + 10.29)(s + 30)}{(s + 1.263)(s + 180)} . \quad (25)$$

Figure 11 gives a typical synthesis of this result. The indicated amplification is necessary because the synthesis of a transfer function by passive elements can only be realized within a gain constant. Table 1 lists the closed-loop specifications and makes a comparison with the closed-loop performances realized by the idealized and modified systems.

Table I
Comparison of the performance realized by the idealized and modified synthesis with the specifications.

Closed-loop Specifications	Idealized System	Modified System
BW $\leq$ 35 rad/sec	30.6	33.5
$K_v \geq 140$ rad/sec	150	150
$\gamma < 35\%$	22	25.8
$t_d < 0.065$ Sec	0.0373	0.0413
*t_r sec	0.0556	0.0546
* ζ	0.707	0.701
* ω_n rad/sec	15	16.22

* Not specified

The figures for the latter system, are calculated values obtained by closing the feedback path on $G_1'(p)$ of equation 24. Ordinarily this need not be done; rather, an estimate of the increase in overshoot is usually satisfactory and sufficiently reliable. For this particular example, the modified closed-loop transfer function is

$$\frac{C(p)}{R(p)} = \frac{122.5 (p + 0.686)}{(p + 5.275)(p + 13.62)(p^2 + 1.52p + 1.17)} . \quad (26)$$

In terms of equation 20 and Figure 2, the zero position is unaltered, a new pole appears at p = -13.62, the pole at (-7) moves to (-5.275), and the radius vectors to the conjugate poles lengthen and rotate toward the imaginary axis. As Table 1 indicates, the added pole tends to produce

small increases in bandwidth, overshoot, and delay time accompanied by a slight decrease in rise time while maintaining a design value of velocity constant.

CONCLUSIONS

The method of system synthesis presented in this paper is based on the extensive variety of transient and steady-state performance characteristics that can be realized with a closed-loop transfer function possessing a conjugate pair of poles, a real pole, and a real zero, with the prior assurance that the poles of the corresponding open-loop transfer function are on the negative real axis. The method is direct and quick, and is sufficiently accurate for many situations normally encountered when unity-feedback is applied to a minimum-phase type I system. Simplicity of the method is achieved by: (1) maintaining a design value of velocity constant, and (2) delaying consideration of the pole-zero excess of the fixed portion of the system $G_2(s)$ until the final step of the procedure. In this way the method is essentially independent of the complexity of $G_2(s)$, and except in marginal situations, the necessity of factoring high degree characteristic equations is avoided. In addition, a simplified RC compensation network can often be realized by the expedient of pole cancellation.

APPENDIX I

The following expressions apply to equation 11:

$$E = \frac{m - k}{k\left[(\zeta - m)^2 + \beta^2\right]} \tag{27}$$

$$F = \frac{m}{k\beta}\left[\frac{(k - \zeta)^2 + \beta^2}{(m - \zeta)^2 + \beta^2}\right]^{1/2} \tag{28}$$

$$\beta = (1 - \zeta^2)^{1/2}$$

$$\psi = \tan^{-1}\frac{\beta}{k - \zeta} - \tan^{-1}\frac{\beta}{m - \zeta} - \tan^{-1}\frac{\beta}{-\zeta} \tag{29}$$

In regard to bandwidth, the square of the magnitude of equation 2 is

$$\left|\frac{C(jy)}{R(jy)}\right|^2 = \left(\frac{m}{k}\right)^2 \frac{k^2 + y^2}{(m^2 + y^2)\left[(1 - y^2)^2 + 4\zeta^2 y^2\right]} . \tag{30}$$

The normalized frequency y at which this equation has a value of 0.5 is the normalized bandwidth BW/ω_n of the closed-loop system. Imposing this condition on equation 30, and letting

$$v = y^2 = (BW/\omega_n)^2 \tag{31}$$

eventually leads to

$$v^3 + (m^2 + c)v^2 + (m^2 c + d)v - m^2 = 0, \tag{32}$$

where

$$c = 4\zeta^2 - 2 \tag{33}$$

and

$$d = 1 - (m/k)^2. \tag{34}$$

The desired normalized bandwidth is then obtained from

$$BW/\omega_n = v^{1/2}, \tag{35}$$

where v is the positive root of equation 32.

REFERENCES

1. Automatic Feedback Control System Synthesis, J. G. Truxal. McGraw-Hill Book Company, Inc., pp 278-316, 1955.

2. Synthesis of Feedback Control Systems by Means of Pole and Zero Location of the Closed Loop Function, M. R. Aaron. AIEE Transactions, vol. 70 pt. II, 1951, pp. 1439-1445.

3. Feedback System Synthesis by the Inverse Root-Locus Method, J. A. Aseltine. IRE Convention Record, vol. 4, pt. 2 - Circuit Theory, pp 13-17, March 1956.

4. Synthesis of Feedback Systems, C. R. Hausenbauer. Ph. D Thesis, Department of Electrical Engineering, University of Missouri, Columbia, Missouri, 1957.

5. Transformation Calculus and Electrical Transients, S. Goldman. Prentice-Hall, Inc., p 62, 1949.

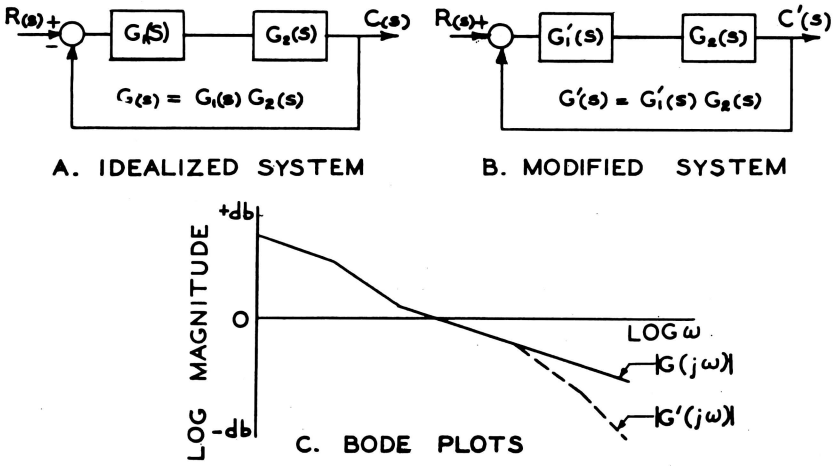

Fig. 1. System block diagrams and Bode plots illustrating the proposed method of system synthesis.

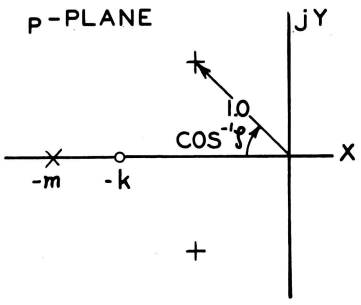

Fig. 2. Pole-zero configuration for equation 2.

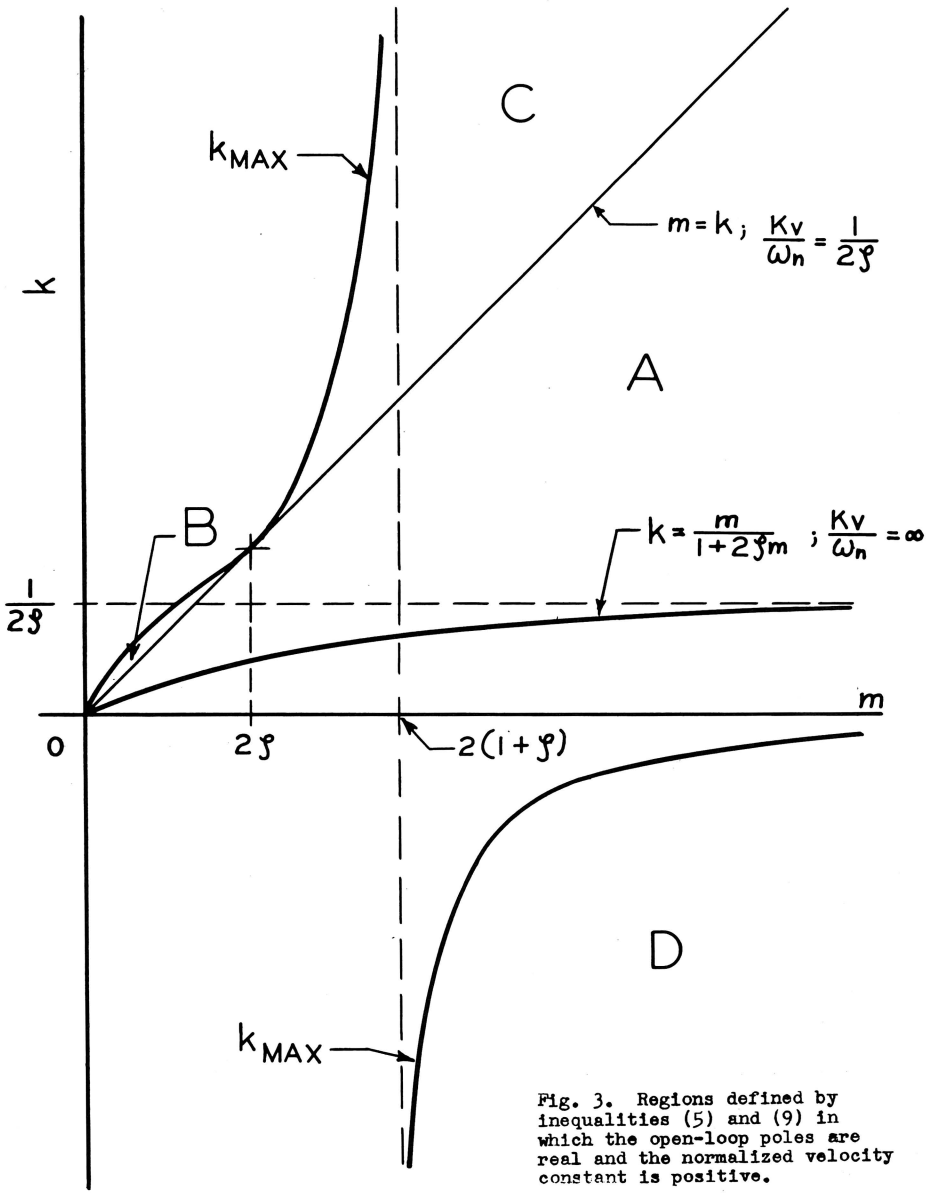

Fig. 3. Regions defined by inequalities (5) and (9) in which the open-loop poles are real and the normalized velocity constant is positive.

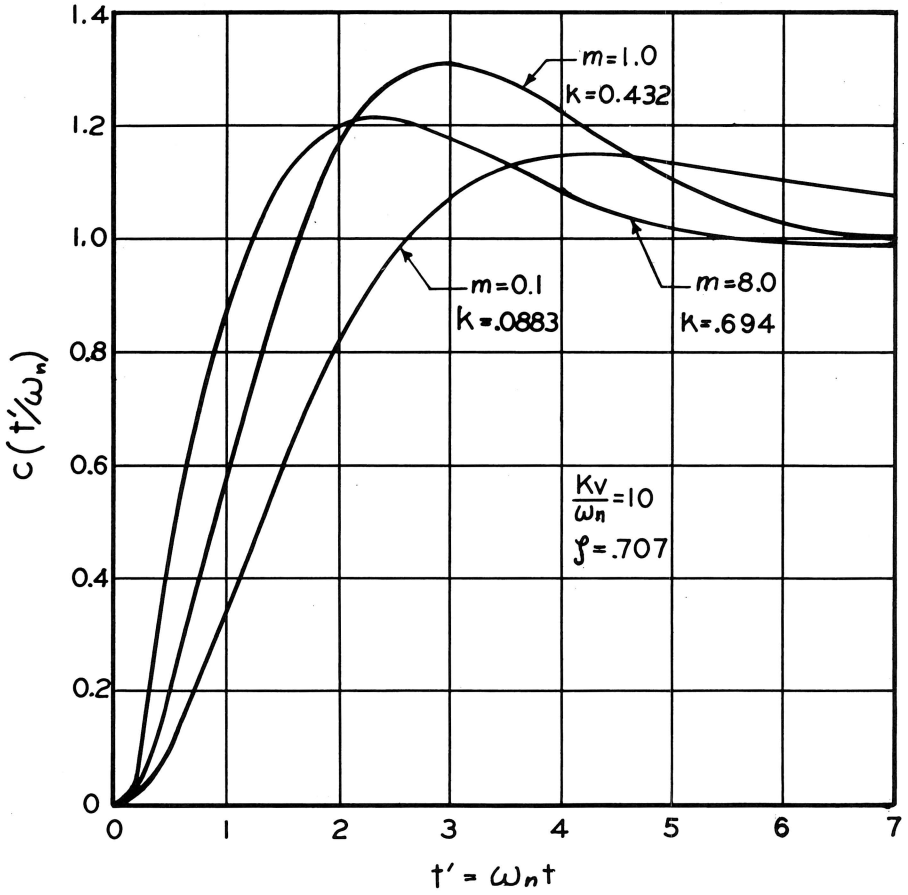

Fig. 4. Closed-loop transient responses to a unit-step-input for several values of m when $K_v/\omega n$ = 10 and ζ = 0.707

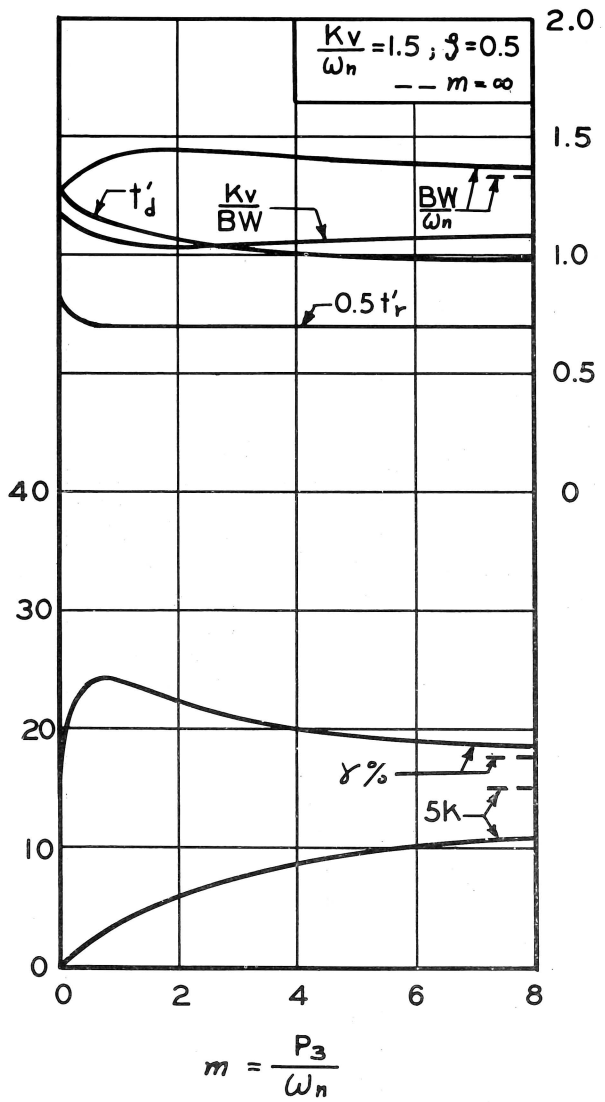

(FIG. 5A)

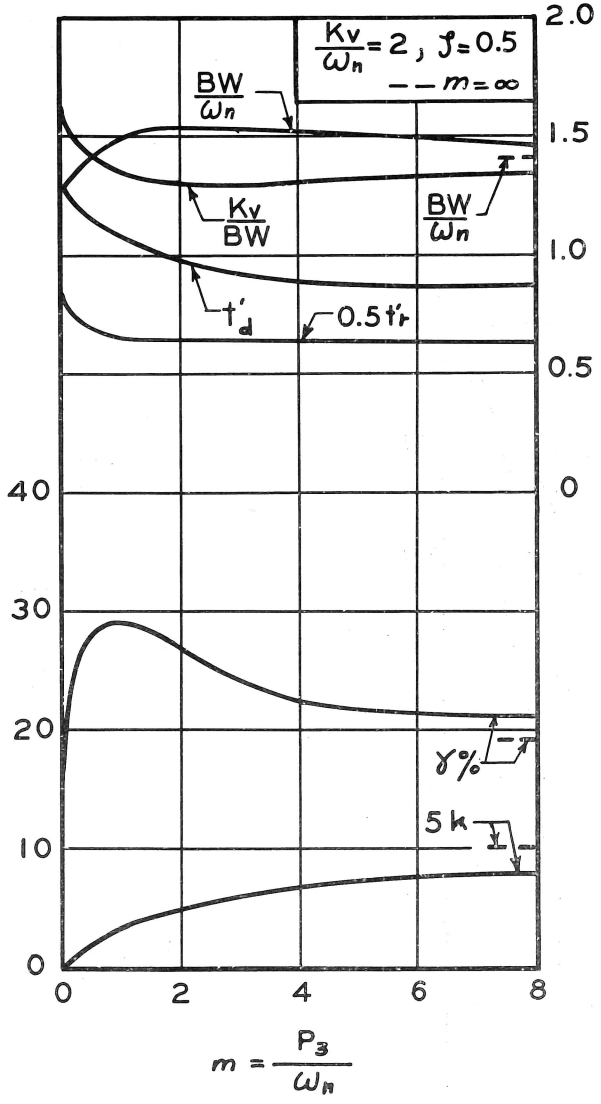

(FIG. 5B)

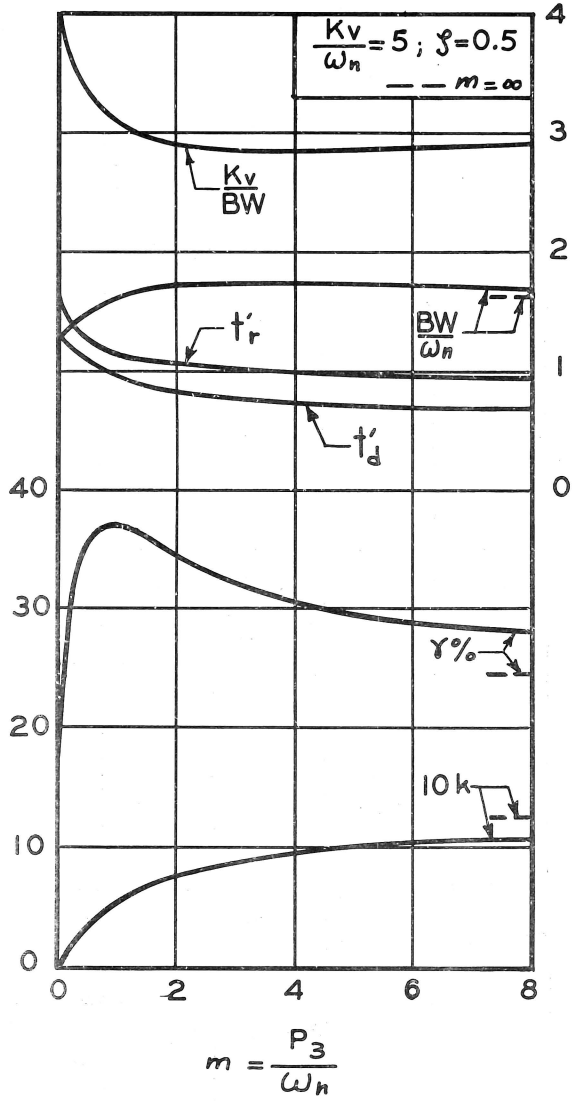

(FIG. 5C)

Fig. 5. A,B,C. Closed-loop performance characteristics when $\vartheta = 0.5$.

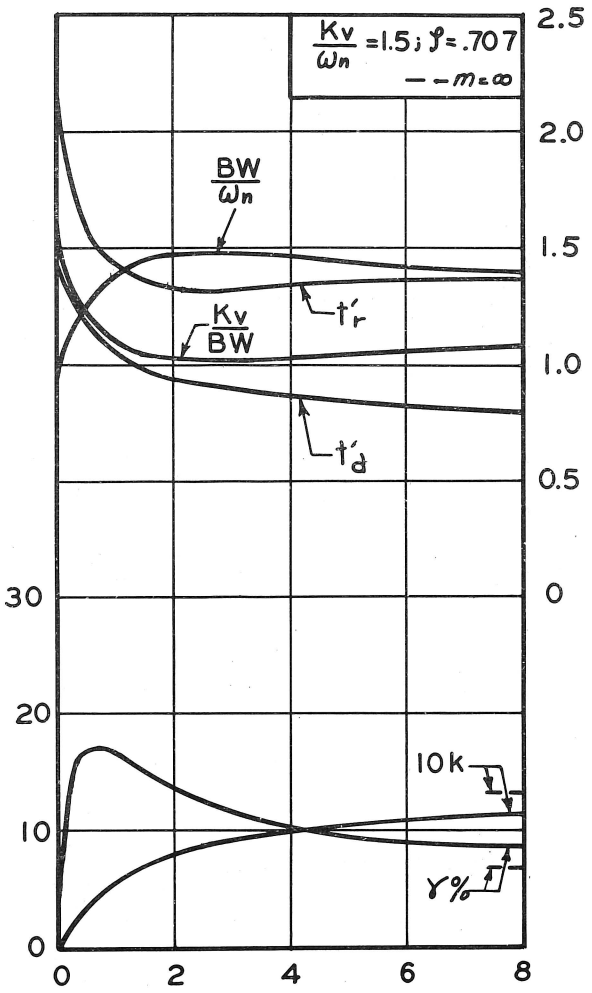

(FIG. 6A) $m = \frac{P_3}{\omega_n}$

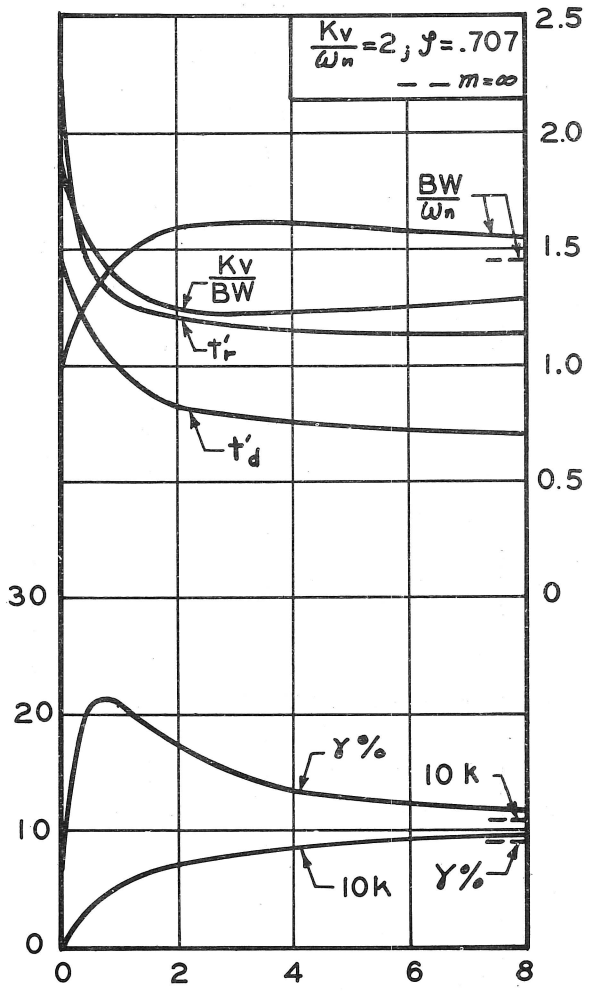

(FIG. 6B) $m = \frac{P_3}{\omega_n}$

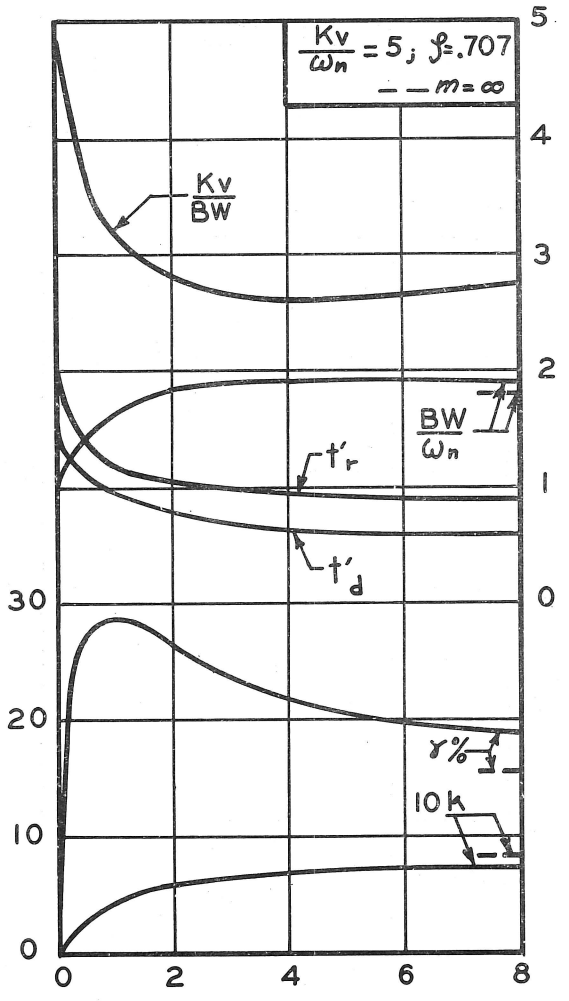

(FIG. 6C) $m = \frac{P_3}{\omega_n}$

Fig. 6, A,B,C,D,E. Closed-loop performance characteristics when $\zeta = 0.707$.

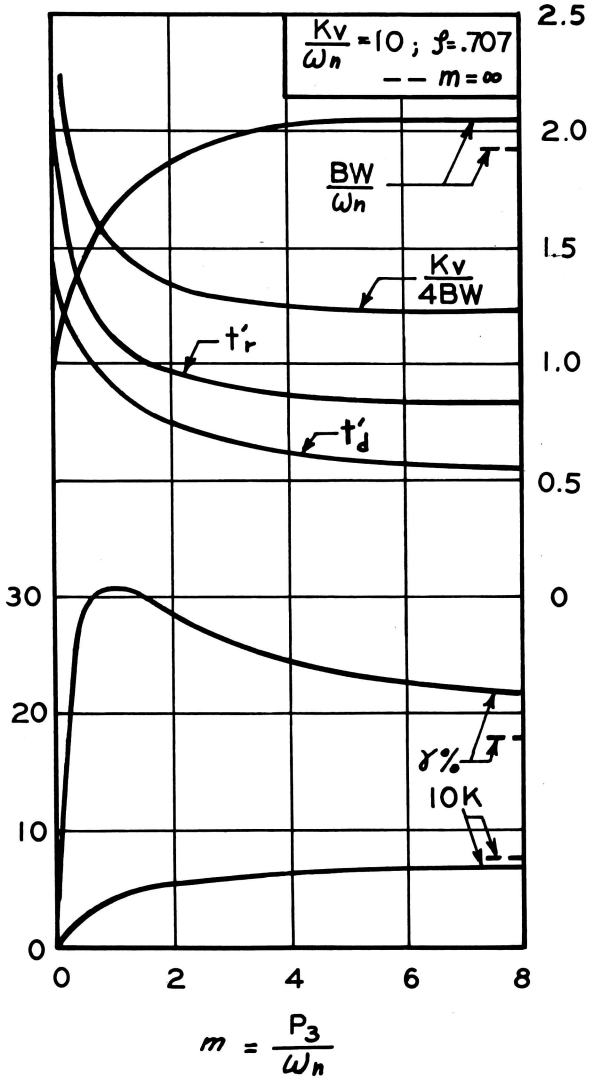

(FIGURE 6D)

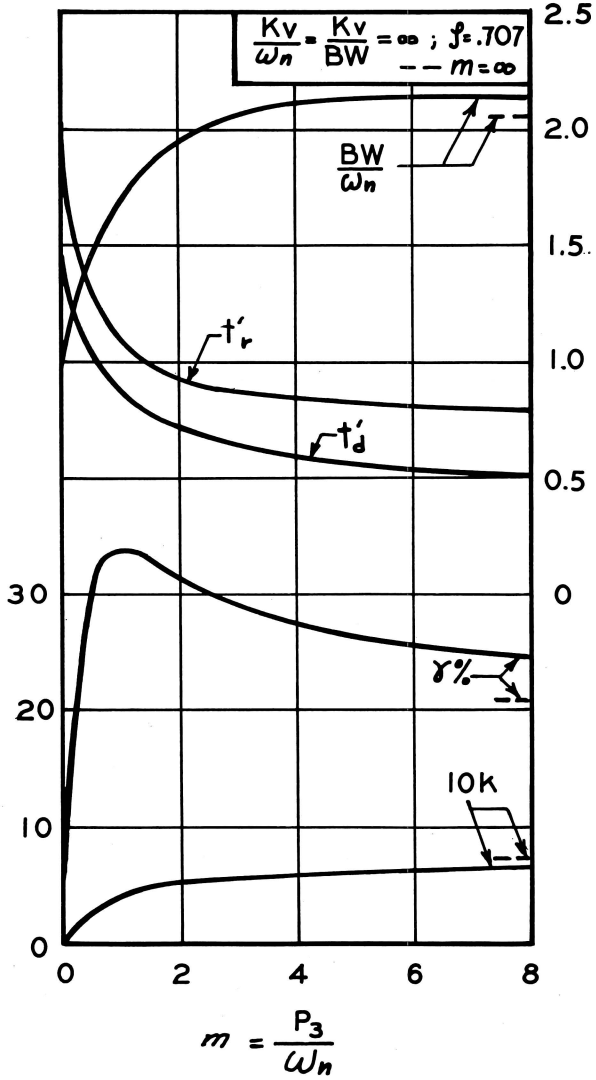

(FIGURE 6E)

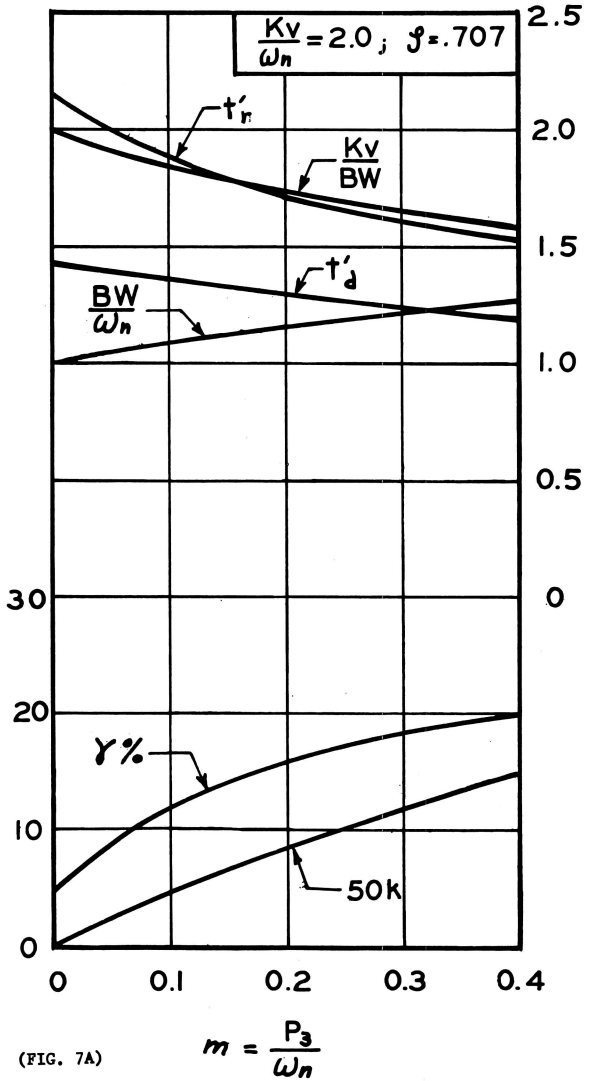

(FIG. 7A)

Fig. 7, A,B,C. Closed-loop performance characteristics for low values of m when $\zeta = 0.707$.

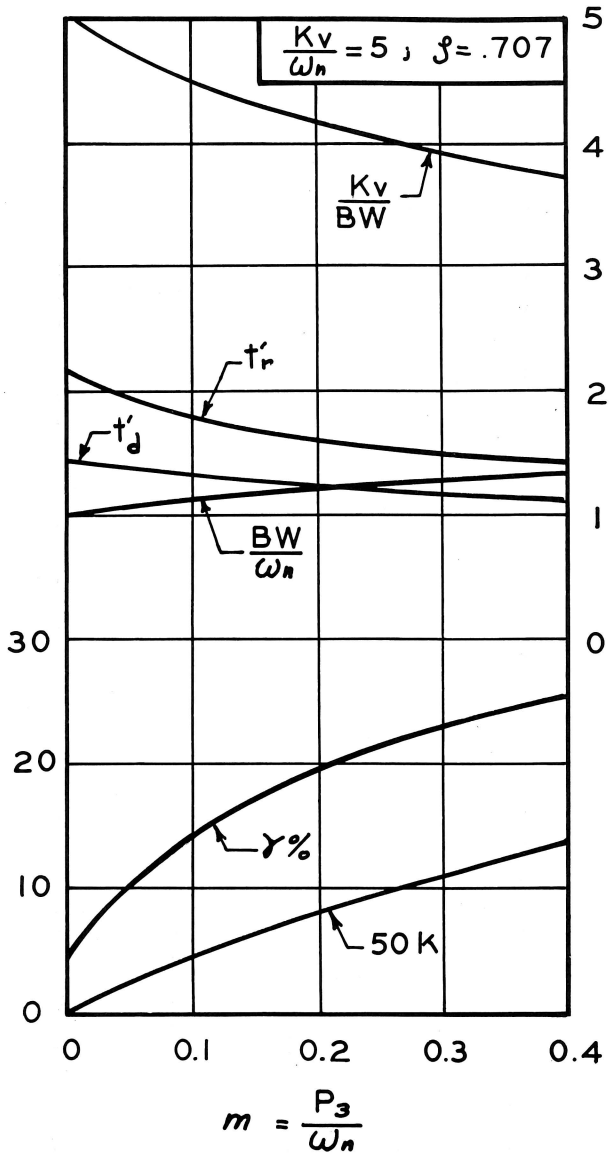

(FIGURE 7B)

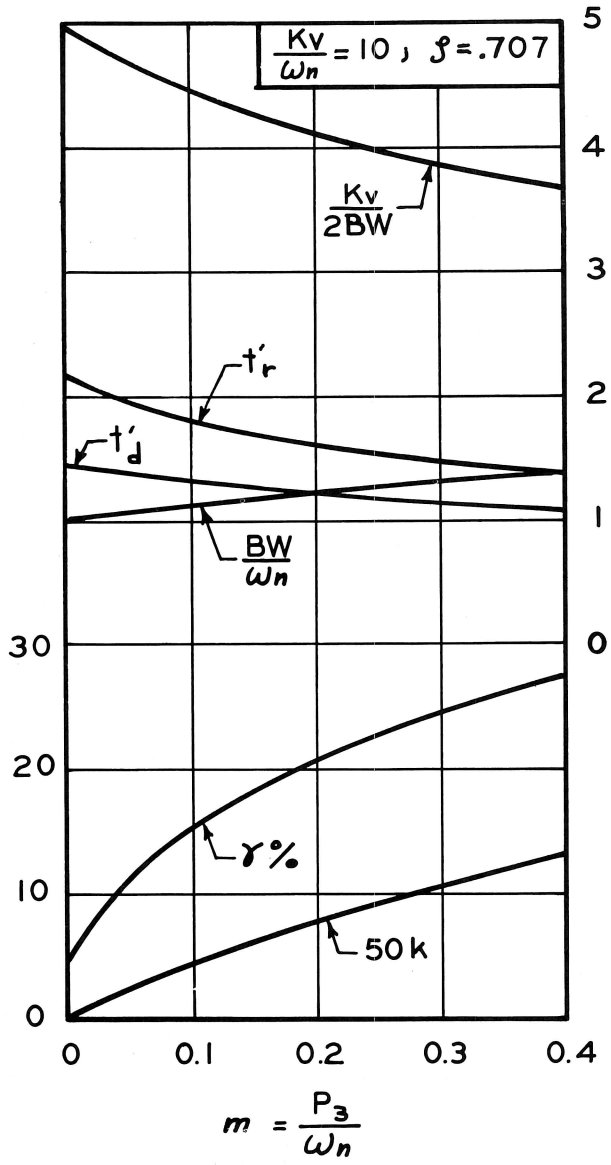

(FIGURE 7C)

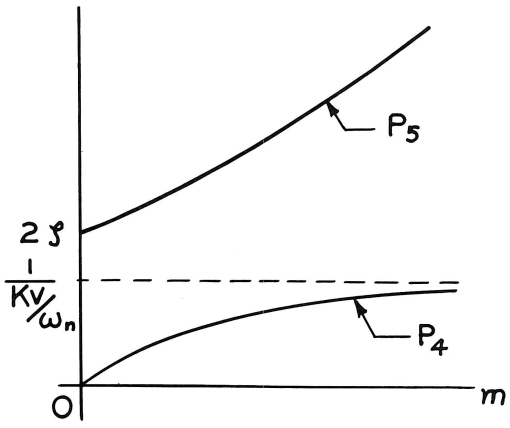

A. POLE MAGNITUDES

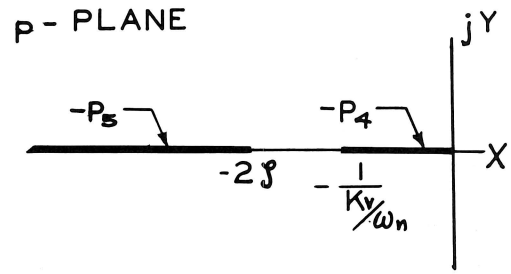

B. POLE LOCI

Fig. 8. Open-loop pole characteristics.

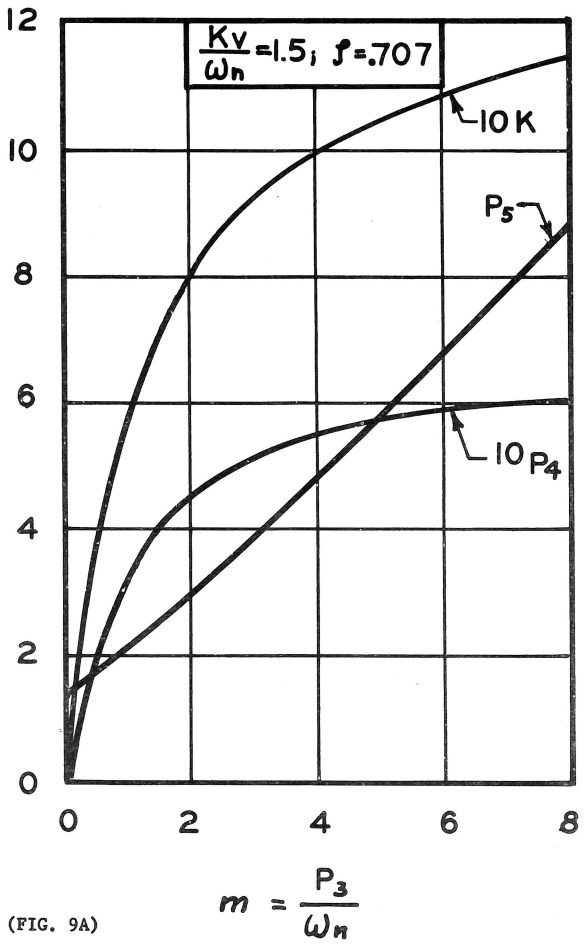

(FIG. 9A)

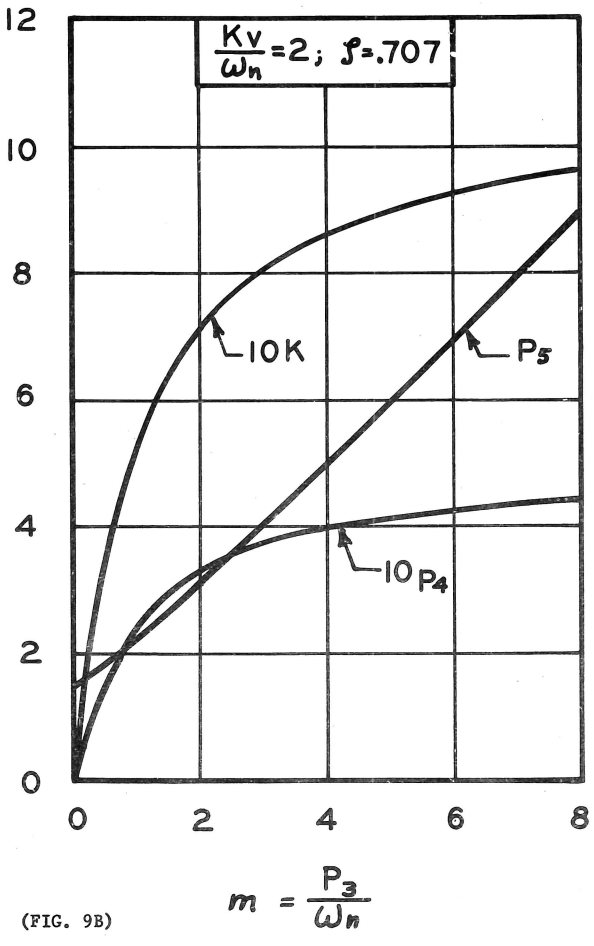

(FIG. 9B)

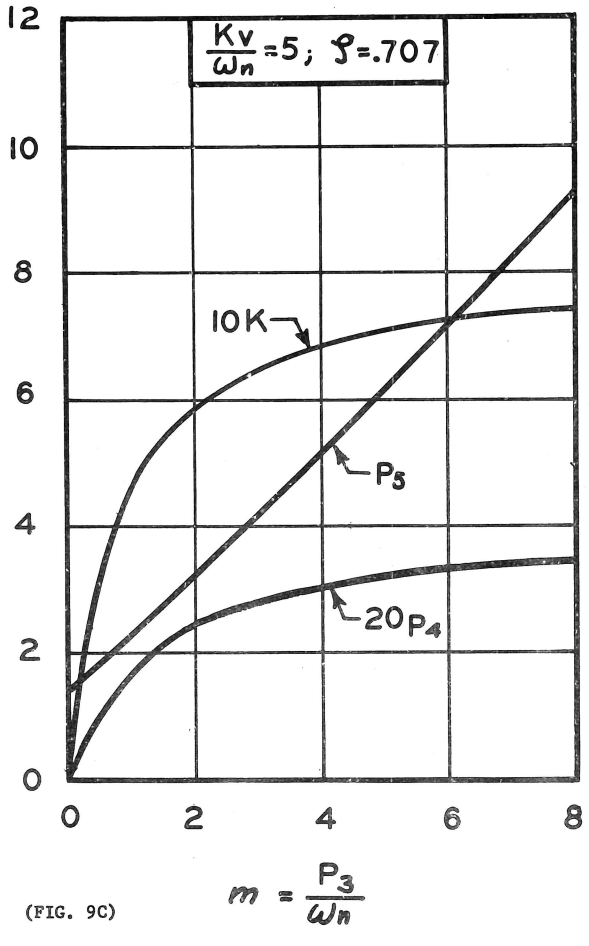

(FIG. 9C)

Fig. 9, A,B,C,D,E. Relationships between open-loop poles and closed-loop real pole and zero when $\zeta = 0.707$.

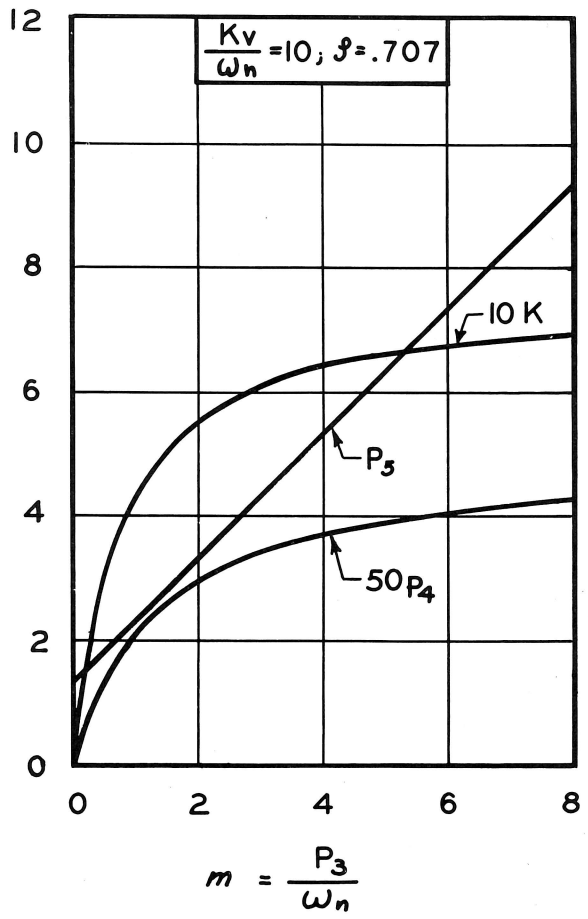

(FIGURE 9D)

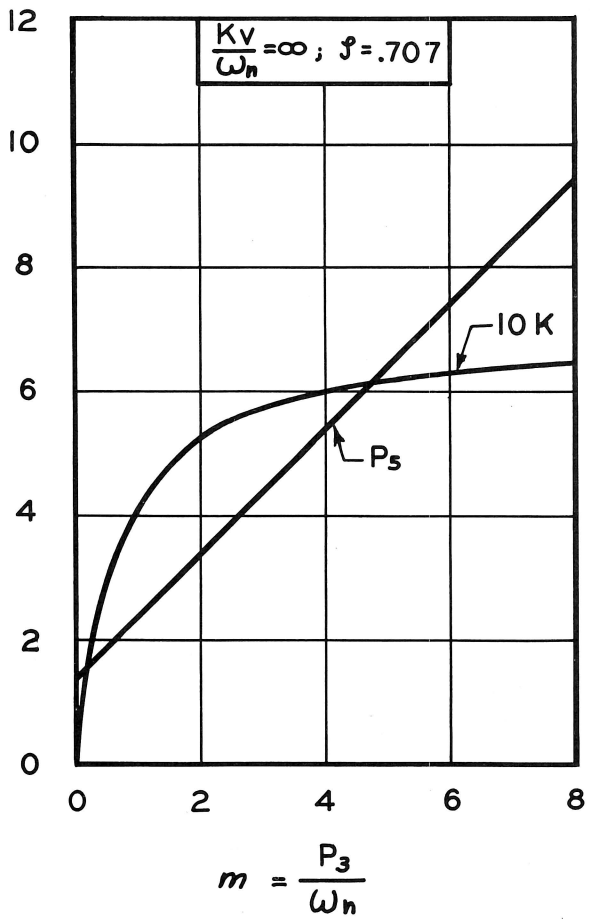

(FIGURE 9E)

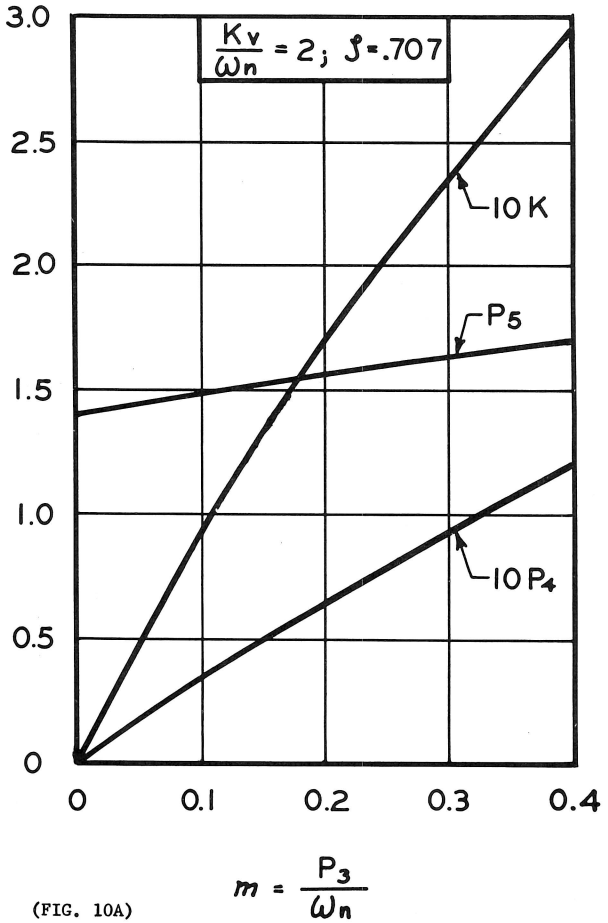

(FIG. 10A)

Fig. 10, A,B,C. Relationships between open-loop poles and closed-loop real pole and zero for low values of m when $\vartheta = 0.707$.

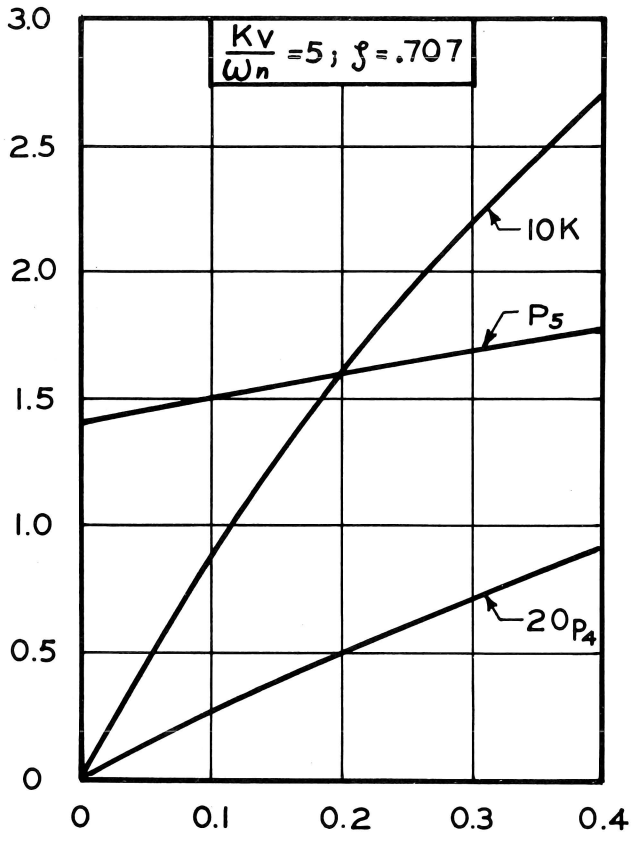

(FIGURE 10B)

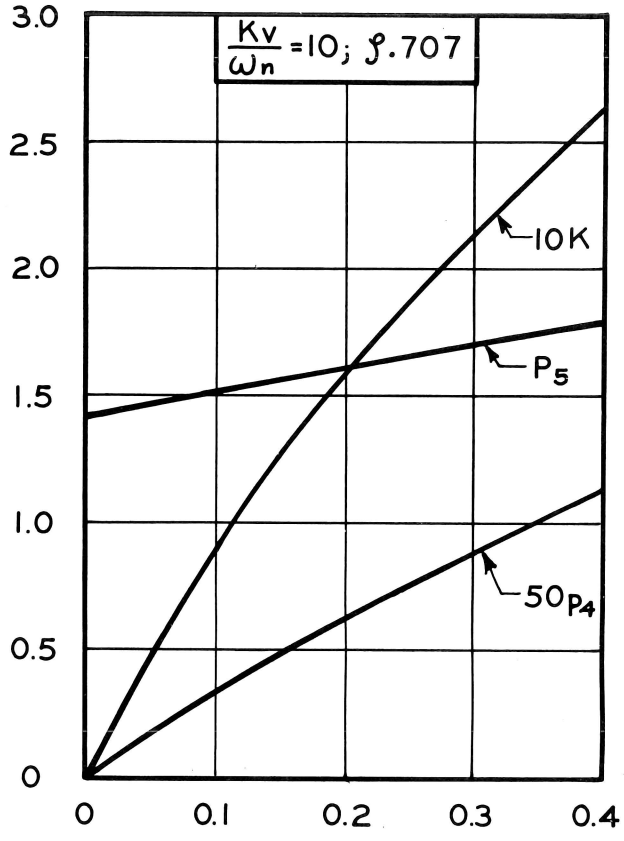

(FIGURE 10C)

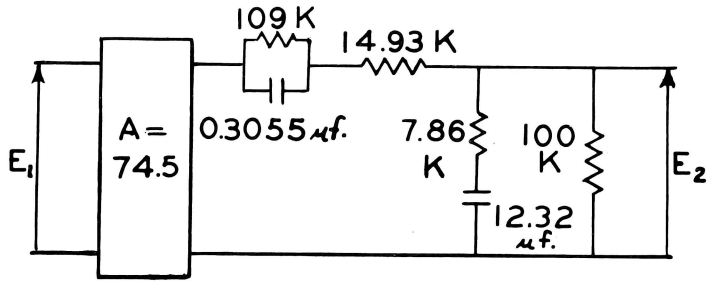

Fig. 11. A typical synthesis of the modified compensation transfer function $G_1(s)$.

PUBLICATIONS OF THE ENGINEERING REPRINT SERIES

Copies of the complete list of publications may be secured from the Director of the Engineering Experiment Station, University of Missouri

Reprint No.

25. Analysis of Single-Phase-to-Three-Phase Static Phase Converters by J. C. Hogan, Associate Professor of Electrical Engineering. Reprinted from Transactions of the American Institute of Electrical Engineers, Vol. 74, p. 403, January, 1956.

26. Enrollment and Incomes in Civil Engineering can be Increased by Harry Rubey, Professor of Civil Engineering. Reprinted from Journal of Engineering Education, Vol. 46, p. 236, November, 1955.

27. A Synthesis Procedure for Sampled-Data Systems by G. V. Lago, Associate Professor of Electrical Engineering. Reprinted from Proceedings of the National Electronics Conference, Vol. 11, p. 251, 1955.

28. Design of Optimum Phase-Shift Oscillators by Donald L. Waidelich, Associate Director, Engineering Experiment Station. Reprinted from Proceedings of the National Electronics Conference, Vol. 11, p. 222, 1955. This article also appeared in Electronics Equipment, Vol. 4, p. 38, April, 1956.

29. Investigation Concerning Polarization in Barium Titanate Ceramics by G. W. Marks, U. S. Navy Electronics Laboratory, Donald L. Waidelich, Associate Director Engineering Experiment Station, University of Missouri and L. A. Monson, U. S. Navy Electronics Laboratory. Reprinted from Transactions of the American Institute of Electrical Engineers, Vol. 75, Part I, p 469, 1956.

30. The Influence of Shank Area on the Tensile Impact Strength of Bolts by John Love, Jr., General Electric Company and O. A. Pringle, Associate Professor of Mechanical Engineering. Reprinted from Transactions of the American Society of Mechanical Engineers, Vol. 78, p 1489, October, 1956.

31. Measurement of Coating Thicknesses by Use of Pulsed Eddy Currents by Donald L. Waidelich, Associate Director, Engineering Experiment Station. Reprinted from Nondestructive Testing, Vol. 14, p 14, May-June 1956.

32. Head Losses in Storm Drain Junction Boxes by Horace W. Wood, Professor of Civil Engineering. Reprinted from Highway Research Board Proceedings, Vol. 35, p 177, 1956.

33. Stability of Laminar Flow in Curved Channels by Chia-Shun Yih, Associate Professor of Engineering Mechanics, University of Michigan and W. M. Sangster, Associate Professor of Civil Engineering, University of Missouri. Reprinted from The Philosophical Magazine, Volume 2, Eighth Series, Page 305, March 1957.

34. Viscosity of Suspensions of Spherical and Other Isodimensional Particles in Liquids by Andrew Pusheng Ting, Chemical Construction Corporation and Ralph H. Luebbers, Professor of Chemical Engineering, University of Missouri. Reprinted from the American Institute of Chemical Engineers Journal, Volume 3, Page 111, March, 1957.

35. Irrigation-Drainage-Climatology for Flat Humid Land by Harry Rubey, Professor Emeritus of Civil Engineering. Reprinted from the Proceedings of the American Society of Civil Engineers, Volume 83, Paper No. 1253, May 1957.

36. The Impedance of a Coil Near a Conductor by D. L. Waidelich, Associate Director, Engineering Experiment Station and C. J. Renken, Jr., Argonne National Laboratory. Reprinted from the Proceedings of the National Electronics Conference, Volume 12, Page 188, 1956.

37. Automatic Control - The Fundamentals by Gladwyn Lago, Associate Professor of Electrical Engineering. Reprinted from the Proceedings of the Second Annual Conference on Automatic Control, University of Oklahoma, April 29-30, 1957, Page 9.

38. Non-Aqueous Solvent Electrochemical Systems, by G. Myron Arcand, Assistant Professor of Chemistry, and James R. Tudor, Assistant Professor of Electrical Engineering. Reprinted from Proceedings of Eleventh Annual Battery Research and Development Conference, Power Sources Division, United States Army, Signal Engineering Laboratories, Fort Manmouth, New Jersey, May 22-23, 1956, pages 16-19.

39. Compensation of Sampled-Data Systems by L. M. Benningfield, Assistant Professor of Electrical Engineering, and G. V. Lago, Associate Professor of Electrical Engineering, Reprinted from Proceedings of the National Electronics Conference, Volume XIII, Hotel Sherman, Chicago, Illinois, October 7, 8, 9, 1957, pages 888-897.

40. A. Application of the Smith Chart to the Design of Microwave Absorbing Materials by D. L. Waidelich, Professor of Electrical Engineering, University of Missouri.
    B. Synthesis of Control Systems Based on an Approximation to a Third-Order System by C. R. Hausenbauer, University of Arizona, Tucson, Ariz., and G. V. Lago, Professor of Electrical Engineering, University of Missouri, Columbia, Mo. A paper presented at the AIEE Summer General Meeting and Air Transportation Conference, Buffalo, N. Y., June 22-27, 1958.

*Out of Print.

The University of Missouri
SCHOOLS AND COLLEGES

College of Arts and Science
School of Social Work
Division of Agricultural Sciences
College of Agriculture
School of Veterinary Medicine
School of Forestry
School of Business and Public Administration
College of Education
College of Engineering
Graduate School
School of Journalism
School of Law
School of Medicine
School of Nursing

University of Missouri Libraries
University of Missouri

MU Engineering Experiment Station Series

Local Identifier Hausenbauer1959

Capture information

Date captured	2018 June
Scanner manufacturer	Ricoh
Scanner model	MP C4503
Scanning software	
Optical resolution	600 dpi
Color settings	Grayscale, 8 bit; Color, 24 bit
File types	Tiff

Source information

Format	Book
Content type	Text
Notes	Digitized duplicate copy not retained in collection.

Derivatives - Access copy

Compression	LZW
Editing software	Adobe Photoshop
Resolution	600 dpi
Color	Grayscale, 8 bit; Color, 24 bit
File types	Tiffs converted to pdf
Notes	Greyscale pages cropped and canvassed. Noise removed from background and text darkened. Color pages cropped.